AGU100 ADVANCING EARTH AND SPACE SCIENCE

Geochemistry, Geophysics, Geosystems

RESEARCH ARTICLE
10.1029/2018GC007477

Special Section:
Carbon Degassing Through Volcanoes and Active Tectonic Regions

Gas Emissions From Volcanoes of the Kuril Island Arc (NW Pacific): Geochemistry and Fluxes

Yuri Taran[1,2], Mikhail Zelenski[3], Ilya Chaplygin[4], Natalia Malik[2], Robin Campion[1], Salvatore Inguaggiato[5], Boris Pokrovsky[6], Elena Kalacheva[2], Dmitri Melnikov[2], Ryunosuke Kazahaya[7], and Tobias Fischer[8]

[1]Institute of Geophysics, UNAM, Coyoacan, Ciudad de Mexico, Mexico, [2]Institute of Volcanology and Seismology FEB RAS, Petropavlovsk-Kamchatsky, Russia, [3]Institute of Experimental Mineralogy RAS, Chernogolovka, Moscow District, Russia, [4]Insitute of Geology of Ore Deposits, Petrography, Mineralogy and Geochemistry, RAS, Moscow, Russia, [5]National Institute of Geophysics and Volcanology, Palermo, Italy, [6]Geological Institute RAS, Pyzhevski 8, Moscow, Russia, [7]Geological Survey of Japan, Tsukuba, Japan, [8]University of New Mexico, Albuquerque, NM, USA

Abstract The Kuril Island arc extending for about 1,200 km from Kamchatka Peninsula to Hokkaido Island is a typical active subduction zone with ~40 historically active subaerial volcanoes, some of which are persistently degassing. Seven Kurilian volcanoes (Ebeko, Sinarka, Kuntomintar, Chirinkotan, Pallas, Berg, and Kudryavy) on six islands (Paramushir, Shiashkotan, Chirinkotan, Ketoy, Urup, and Iturup) emit into the atmosphere > 90% of the total fumarolic gas of the arc. During the field campaigns in 2015–2017 direct sampling of fumaroles, MultiGas measurements of the fumarolic plumes and DOAS remote determinations of the SO_2 flux were conducted on these volcanoes. Maximal temperatures of the fumaroles in 2015–2016 were 510°C (Ebeko), 440°C (Sinarka), 260°C (Kuntomintar), 720°C (Pallas), and 820°C (Kudryavy). The total SO_2 flux (in metric tons per day) from fumarolic fields of the studied volcanoes was measured as ~1,800 ± 300 t/d, and the CO_2 flux is estimated as 1,250 ± 400 t/d. Geochemical characteristics of the sampled gases include δD and δ^{18}O of fumarolic condensates, δ^{13}C of CO_2, δ^{34}S of the total sulfur, ratios ^{3}He/^{4}He and ^{40}Ar/^{36}Ar, concentrations of the major gas species, and trace elements in the volcanic gas condensates. The mole ratios C/S are generally <1. All volcanoes of the arc, except the southernmost Mendeleev and Golovnin volcanoes on Kunashir Island, emit gases with ^{3}He/^{4}He values of >7R_A (where R_A is the atmospheric ^{3}He/^{4}He). The highest ^{3}He/^{4}He ratios of 8.3R_A were measured in fumaroles of the Pallas volcano (Ketoy Island) in the middle of the arc.

Key Points:
- The SO_2 flux was for the first time measured from the whole Kuril Island arc
- The average molar C/S ratio for the Kuril arc fumaroles is <1, and the CO_2 flux is comparable with the SO_2 flux
- 3He/4He ratios in fumarolic gases are >7Ra except the southernmost Kunashir Island

Correspondence to:
Y. Taran,
taran@geofisica.unam.mx

Citation:
Taran, Y., Zelenski, M., Chaplygin, I., Malik, N., Campion, R., Inguaggiato, S., et al. (2018). Gas emissions from volcanoes of the Kuril Island arc (NW Pacific): Geochemistry and fluxes. *Geochemistry, Geophysics, Geosystems*, *19*. https://doi.org/10.1029/2018GC007477

Received 7 FEB 2018
Accepted 30 APR 2018
Accepted article online 8 MAY 2018

1. Introduction

The Kuril Island arc stretches over ~1,200 km from Kamchatka Peninsula to Hokkaido Island and separates the marginal Sea of Okhotsk from the Pacific Ocean (Figure 1). The Pacific plate is subducting beneath the arc with a velocity of 8–9 cm/yr and close to the trench has Cretaceous age (e.g., Avdeiko et al., 2002; Bailey, 1996; Dreyer et al., 2010). The thickness of the oceanic sediments before the trench, according to the DSDP drillings is >300 m (e.g., Bailey, 1993, 1996). There are ~40 of the Holocene volcanic edifices on the arc (Fedorchenko et al., 1989; Gorshkov, 1970, among others), many of which are historically active, and at least three were in eruption in 2015–2017. Many volcanoes of the arc are persistently degassing, but to the best of our knowledge only seven of them have long-lived fumarolic fields with high-temperature (>250°C) fumaroles. These are (from north to south): Ebeko (Paramushir), Sinarka and Kuntomintar (Shiashkotan), Pallas (Ketoy), Berg (Urup), Chernogo (Black Brothers), and Kudryavy (Iturup). Most of the other degassing volcanoes host volcano-hydrothermal systems with boiling-point steam vents (e.g., Golovnin and Mendeleev [Kunashir] and Baransky [Iturup]). The others like Fuss and Chikurachki (Paramushir), Alaid (Atlasov), Sarychev (Matua), Chirinkotan, and Grozny (Iturup) demonstrate a short-lived gas activity after eruptions or during the repose periods between the eruptions.

The studies of the geochemistry of volcanic gases of the Kuril arc have started with a decade of the monitoring of fumaroles of Ebeko volcano by Menyailov et al (1985). Menyailov et al. (1986) reported data on the composition of a high-temperature gas sampled immediately after the 1981 eruption of Alaid volcano. Taran (1992) reported analyses of low-temperature gas vents (140–150°C) from Kuntomintar (Shiashkotan) and Rasshua volcanoes. The most detailed geochemical studies have been conducted at Kudryavy volcano

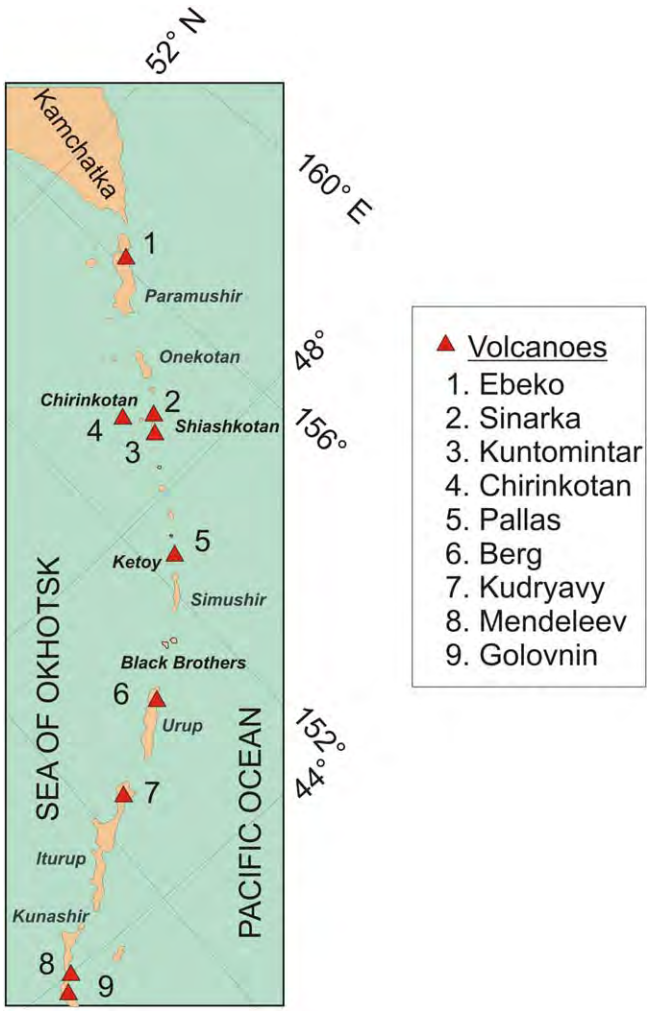

Figure 1. Kuril Island arc. Red triangles are volcanoes studied in this work.

(Iturup Island), where the highest temperature of fumaroles ever measured (940°C) have been recorded in 1992 (Korzhinsky et al., 1993; Tkachenko et al., 1992). Because of its relative accessibility, this volcano became an object of comprehensive studies of many geochemical aspects of the magmatic degassing including trace element geochemistry, sublimate mineralogy, origin of magmatic fluid, and the SO_2 flux (Botcharnikov et al., 1998, 2003; Fischer et al., 1998; Korzhinsky et al., 1994; Taran et al., 1995; Wahrenberger et al., 2002; Yudovskaya et al., 2008, among others).

Terrestrial remote measurements of the SO_2 flux from the Kurilian volcanoes are limited to a study by Fischer et al. (1998) at Kudryavy volcano in 1995 where the flux of 75–100 t/d was reported. Recently, Carn et al. (2017) published the first data on the global volcanic SO_2 emission derived from the satellite measurements made during the 2005–2015 decade by the Ozone Monitoring Instrument (OMI). Their data base includes fluxes from four Kurilian volcanoes of both eruptive and passive degassing. Taran (2009) made an attempt to estimate the total magmatic volatile output from the whole Kamchatka-Kuril subduction zone by comparing visually observed volcanic plumes with a limited number of plumes that have been measured instrumentally.

Here we report new data on the chemical and isotopic composition of volcanic gases and the SO_2 flux from seven volcanoes of the Kuril arc. Gas emissions from five volcanoes, Sinarka and Kuntomintar on Shiashkotan Island, Chirinkotan volcano-island, Pallas on Ketoy Island, and Berg on Urup Island, were studied for the first time. We estimate that these seven passively degassing volcanoes emit $\geq$90% of the fumarolic gas from the Kuril arc, and therefore, their noneruptive SO_2 flux is representative for the whole arc.

2. Sampling and Measurement Locations

2.1. Ebeko Volcano, Paramushir Island

Ebeko volcano (1,030 m asl; 50°41′N, 156°01′E) is located at the northern part of Paramushir Island, at the north of Vernadsky Ridge (Figure 2) and is composed of several Quaternary volcanic cones. The Neogene volcano-clastic basement occurs below ~200 m asl (Melekestsev et al., 1993). The postglacial cone of Ebeko is composed of lava flows and pyroclastics of andesitic composition. The summit is represented by three craters: Northern, Middle, and Southern (Figure 2c). The modern phreatic and fumarolic activity of Ebeko started after a strong explosive phreatic-magmatic eruption from the Middle crater in 1934–1935 (Gorshkov, 1970; Melekestsev et al., 1993). A short review of the phreatic activity of the volcano since that event can be found in Kalacheva et al. (2016). The last eruption started on October 2016 and is lasting up to date (August 2017). A specific feature of the Ebeko fumarolic activity is the presence of three distinct types of fluids: (i) a high-temperature vent (520°C, August 2015) that opened in 2011 (Kotenko et al., 2012) with a typical "arc magmatic" composition; (ii) low-temperature vents (98–120°C) with a high HCl content (up to 0.6 mol %); (iii) low-temperature vents (~100°C) with almost no HCl. Sampling of the fumaroles has been conducted in September 2015. Here we report our geochemical data on three representative fumarolic vents with different temperatures and the Cl content. The SO_2 flux from the high-temperature vent (Active Funnel) was measured in August 2015 and July–August 2017. In September 2015, it was a stationary, highest-temperature fumarole on the field, and in 2017 the SO_2 flux measurements were conducted during short periods between steam-ash emissions.

2.2. Chirinkotan

Chirinkotan (680 m asl; 48°58′4″N, 153°29′08″) is a back arc volcano, about 45 km to the west from Shiashkotan. This is a small volcanic island, ~3 × 3 km^2, 680 m asl, rising from about 2,000 m depth. Its ~1 km-

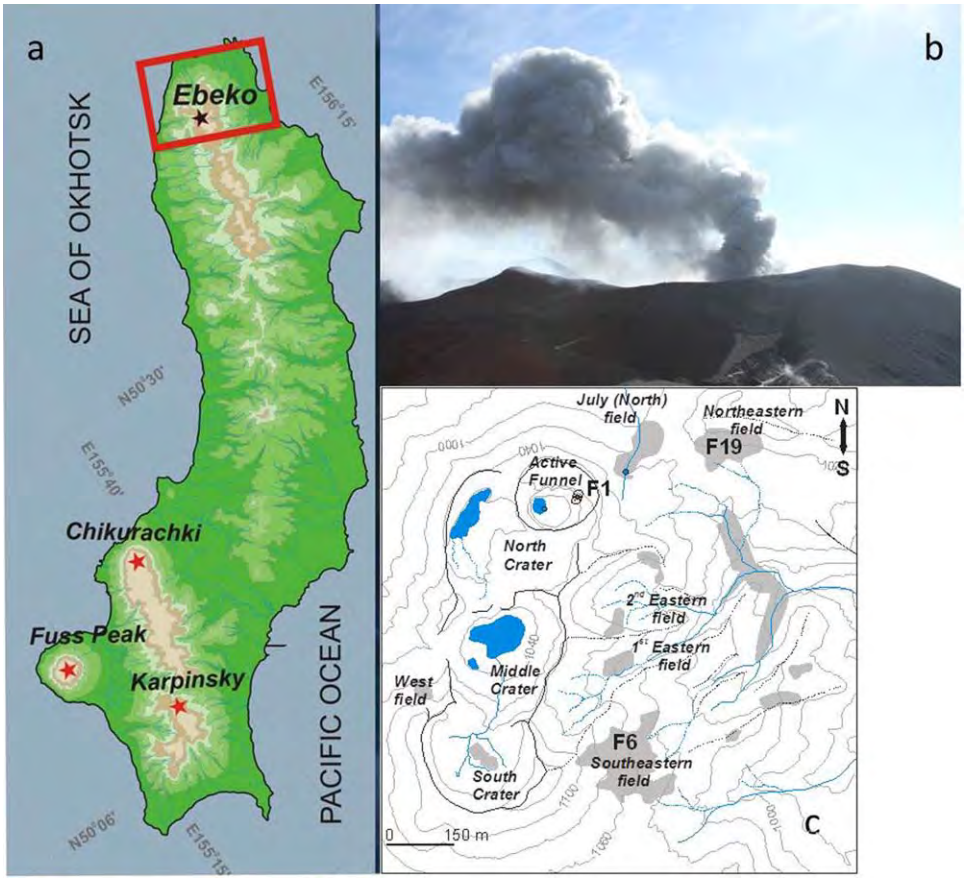

Figure 2. (a) Ebeko volcano on Paramushir Island. (b) Typical ash-steam plume in the summer 2017, photo Ilia Chaplygin. (c) Map of the summit part of Ebeko volcano with fumarolic fields (gray spots) and sampling points as in Table 1.

wide crater with an active growing dome is open to the south (Figure 3). The volcano is active since 2013 with episodic steam-ash explosions and a permanent steam plume between explosions. It was impossible to climb down the crater in August 2015, a few days after a strong explosion, but a loud whistling noise and a dense plume from the dome were annotated (Figure 3c). The last strong explosion with the ash cloud risen up to 8.5 km occurred in November 2016 (Rybin et al., 2017).

2.3. Sinarka and Kuntomintar Volcanoes, Shiashkotan Island

Sinarka (934 m asl; 48°52′29.44″N and 154°10′13.66″E) and Kuntomintar (828 m asl, 48°45′32.22″N and 154°0′46.16″E) stratovolcanoes compose the Shiashkotan Island (Figure 4). The distance between summits of Sinarka and Kuntomintar is ~18 km. According to Gorshkov (1970) and Stratula (1969), Sinarka is a complex stratovolcano of the Somma-Vesuvius type with old caldera walls and a young andesitic extrusive dome actively degassing since 1878 (Gorshkov, 1970). The fumarolic field is located at the northern sector of the edifice, on steep (20°–30°) slopes of the young dome up to the summit (Figure 4a). The field has a dimension of approximately 120 × 250 m^2, extending in an S-N direction between 800 and 930 m asl. The maximum measured temperature of 441°C was found at the upper part of the dome. Several fumarolic vents are located along a fracture on the N-slope of the upper dome up to the summit (Figure 4e).

The hydrothermally active crater of Kuntomintar is a large amphitheater opened to NW with an eroded former crater of the direct blast with highly altered crater walls (Gorshkov, 1970; Stratula, 1969). The last eruption occurred in 1872 (Gorshkov, 1970; Markhinin & Stratula, 1977). Fumarolic activity is spread within the amphitheater and the field can be approximated by an ellipse ~400 × 700 m^2 at the elevations from 300 to 800 m asl (Figures 4b and 4d). Most of the fumarolic vents are located in the lower part of the circus. The highest temperature in August 2016 of 260°C was measured in the middle of the field at the elevation of

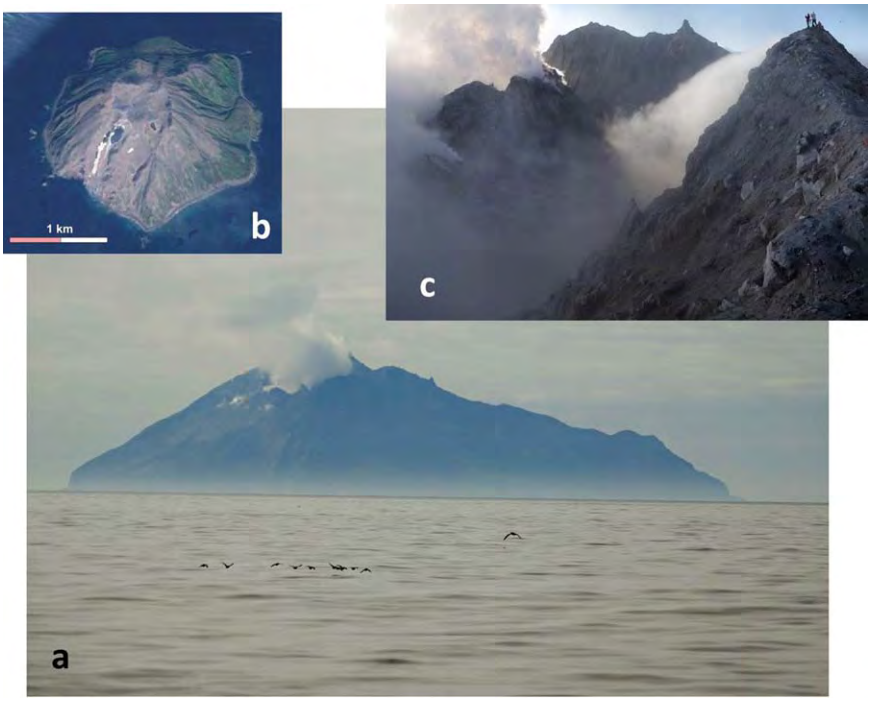

Figure 3. (a) Chirinkotan Island in July 2016 (Photo Y. Taran) and (b) its Google map image. View inside the crater of Chirinkotan in August 2015. Photo O. Chaplygin.

480 m asl. Here we performed a direct sampling of six fumarolic vents and several MultiGas traverses. The SO_2 flux was measured at the distance of about 500 m from the lowest fumarolic vents.

2.4. Pallas Volcano, Ketoy Island

Pallas volcano (928 m asl, 47°20′36″N, 152°28′46″E) is one of the eruption centers at the summit part of Ketoy Island. This is a cinder cone with a ~130 m deep crater filled with acid (pH 2.5) and now cold (12°C) lake. A powerful fumarolic field is situated on the NE slope of the cone at elevations 700–880 m asl (Figure 5). The field dimensions are approximately 180 × 400 m^2. At the lower part of the field, the temperatures of fumaroles vary from 95 to 440°C. Maximal fumarolic temperature at the upper part of the field reaches 720°C. Fumarolic vents with temperatures <150°C are incrusted with elemental sulfur; some sulfur cones reach up to 2 m height. Many sulfur towers and sulfur flows with a thickness 0.5–1 m and a length of up to 100 m are observed in the lower part of the field. The direct sampling of six fumarolic vents, several MultiGas profiles and the SO_2 flux measurements were performed here.

2.5. Berg Volcano, Urup Island

Berg volcano is a lava dome inside a 2 km-wide caldera that is breached to the North-West. It belongs to a group of three small stratovolcanoes known as the Kolokol Volcanic Group, in the central portion of Urup Island (Figure 6). Reconnaissance work carried out in the seventies showed that it has a long-term fumarolic activity from the summit area (Chirkov et al., 1972), but neither sampling nor measurements have been ever performed due to the remoteness of the volcano. On 6 August 2017, the dome was reached after a 2 days long approach march. Significant morphological changes were observed compared to aerial and satellite images taken during the years 1990s and 2000s, including five new phreatic craters filled with lakes or snow that are located to the south of the dome. These new craters together with the occurrence of vegetation recently killed by the gases on the NW flanks of the volcano, suggests a recent change of the activity and degassing of the volcano. Only low-temperature fumaroles on the extrusive dome were accessible at Berg volcano. We performed also measurements of the SO_2 flux, MultiGas probing and filter-pack pumping from the crater rim.

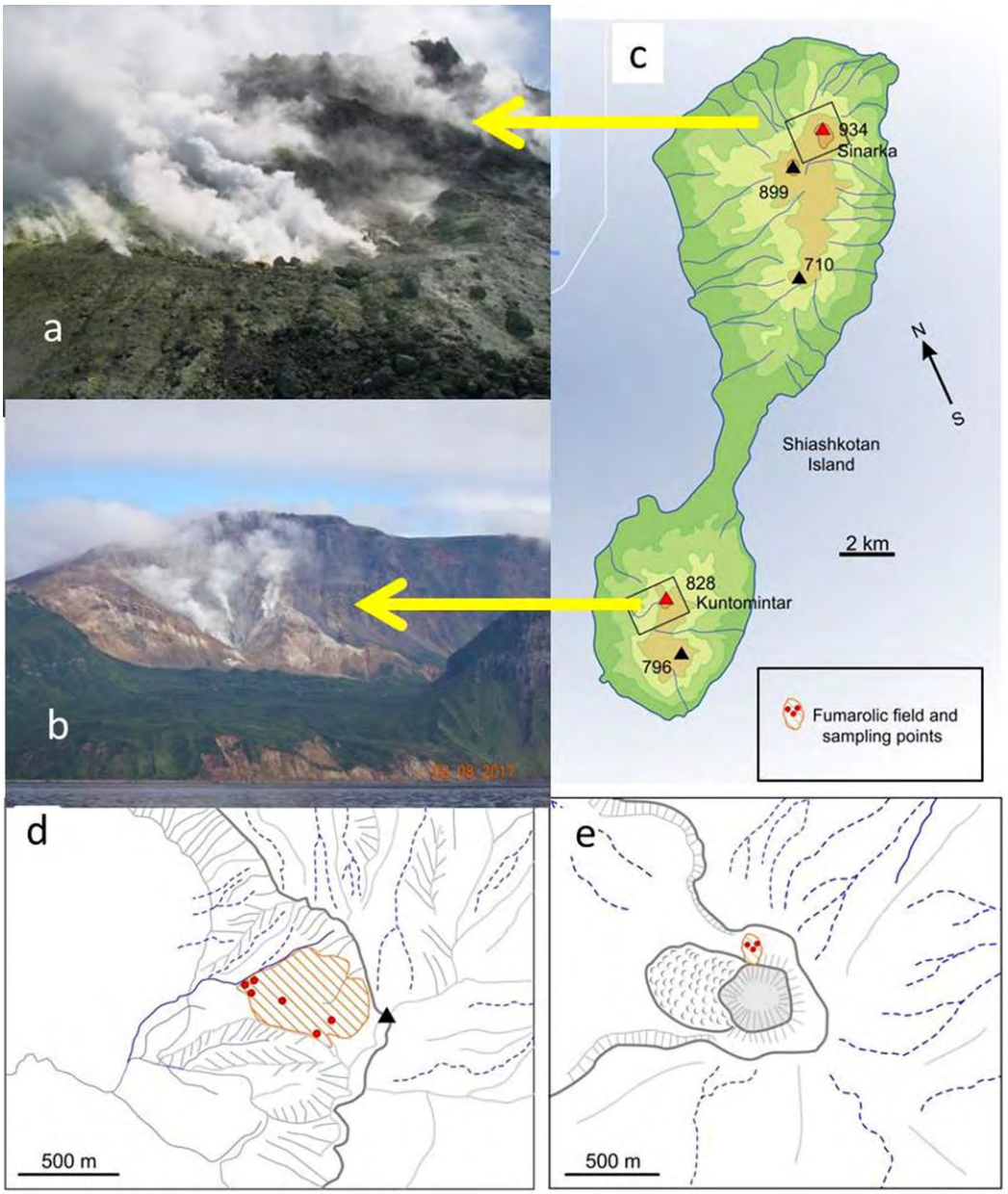

Figure 4. (a, b) Fumarolic fields of (a) Sinarka and (b) Kuntomintar volcanoes on Shiashkotan Island. Photo Mikhail Zelenski and Elena Kalacheva. (c) Map of Shiashkotan Island with locations of Sinarka and Kuntomintar volcanoes. (d, e) Sketch maps of the craters ((d) Kuntomintar and (e) Sinarka) with locations of the fumarolic gas sampling points.

2.6. Kudryavy Volcano, Iturup Island

Kudryavy is a 986 m asl Holocene stratovolcano inside the Medvezhia caldera at the north of Iturup Island (Figure 7). The last magmatic eruption of the volcano with a short lava flow of basaltic andesite composition occurred in 1883 (Gorshkov, 1970). Many papers have been published about Kudryavy volcano starting with Tkachenko et al. (1992). In 2015–2017, the morphology of the crater and locations of main fumarolic vents have not changed since the phreatic eruption in 1999, when a new small crater was formed with a vigorous fumarole at its bottom, ~50 m deep, with temperature >800°C (i.e., Chaplygin et al., 2016). All fumarolic temperatures in 2015–2017 were <900°C. Two fumaroles were sampled in 2016 with the temperature of 780 and 590°C. The SO_2 flux was measured in August 2016 and August–September 2017.

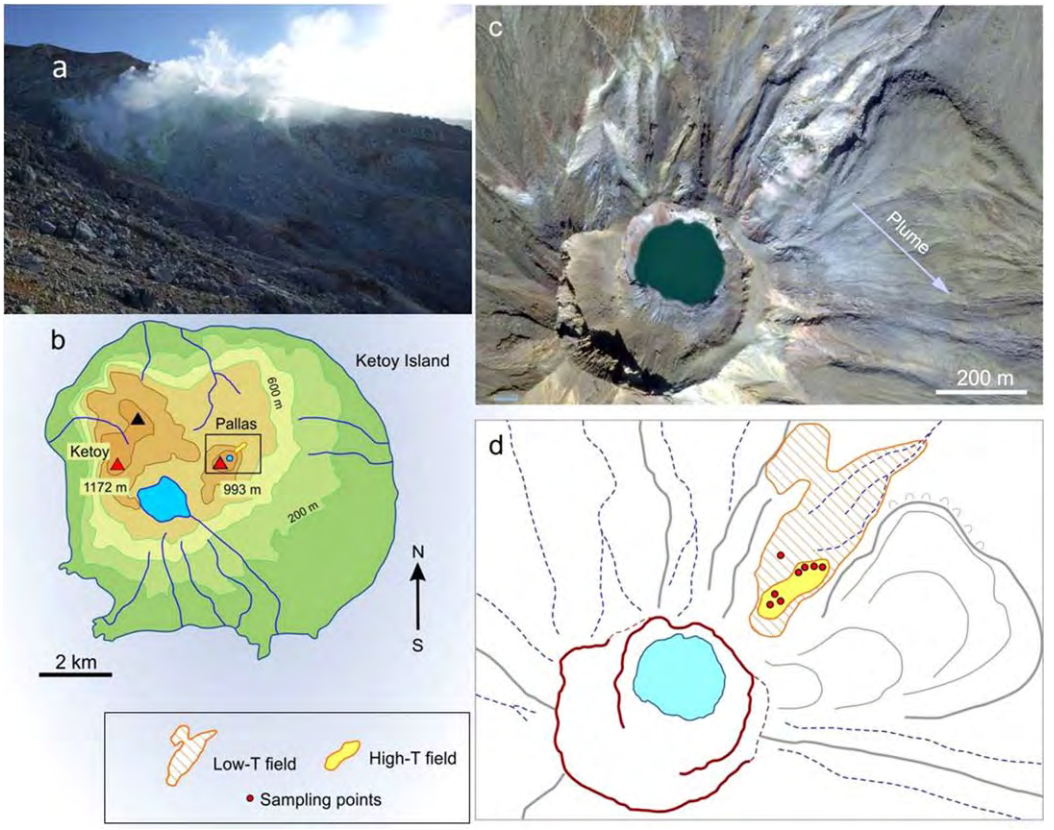

Figure 5. (a) Fumarolic field of Pallas volcano on Ketoy Island. Photo Ilia Chaplygin. (b) Map of Ketoy Island with location of Pallas volcano. (c) Google map image of the Pallas cone with Glazok Lake and fumarolic field. (d) Location of the fumarolic gas sample sites.

3. Methods

3.1. Sampling and Analysis

Fumarolic gases were sampled for chemical and isotopic composition, vapor condensates for δD and δ^{18}O and major and trace element composition. At each site separately were taken samples for H_2S fixation in bubblers with 10% of Cd-acetate and dry gas for δ^{13}C in CO_2. Gases for general analysis were sampled through a quartz tube inserted into the fumarolic vent. Sampling tubes were connected with Giggenbach bottles filled with 40–100 mL of 4 N NaOH solution. Condensates and H_2S were sampled in series of two-three bubblers cooled by snow or using a glass condenser cooled by water. Dry gas was sampled into 10 mL vacuntainers. Headspace gases from Giggenbach bottles and dry gas from vacutainers were analyzed by gas chromatograph techniques on Gow-Mac 580 instrument with molecular sieves and Porapak Q packed columns and He and Ar as carrier gases. Ar was determined using a CT3-Althech composite column at room temperature. The analytical error was ~5%. Alkaline condensates after oxidation by H_2O_2 were analyzed for F, Cl, SO_4, and CO_2 according to Giggenbach and Goguel (1989). Concentration of SO_2 was calculated as a difference between the total sulfur from alkaline condensates and concentration of H_2S calculated from the amount of precipitated CdS and a measured amount of the condensate. Oxidized alkaline condensates were used for precipitation of $BaSO_4$ for the isotopic analysis of the total sulfur.

Concentrations of trace elements were determined by ICP-MS (Agilent 7500 CE) in the Geological Department of the Moscow State University. All determinations were performed with the external standard calibration method, using Re and In as the internal standards. The accuracy of the results (±5%) was compared against certified reference materials (NRCSLR-4, SPS-SW1, and NIST-1643e).

Isotopic composition of volcanic gas condensates (δD and δ^{18}O expressed as ‰ versus V-SMOW) was analyzed at the Institute of Volcanology and Seismology (Kamchatka, Russia) using Los Gatos analyzer with

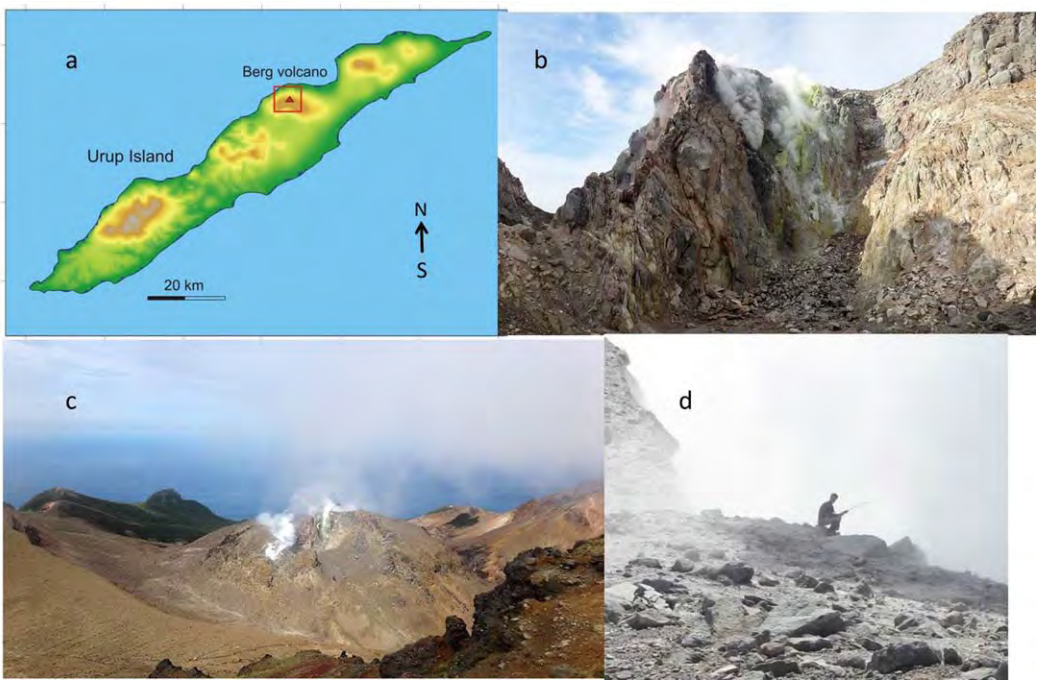

Figure 6. (a) Urup Island and location of Berg volcano. (b, c) Fumarolic fields at Berg volcano. Photo Denis Veselov. (d) Measurements by MultiGas at the crater rim of Berg volcano. Photo I. Chaplygin.

analytical errors 1‰ for δD and 0.1‰ for δ^{18}O. The δ^{13}C of CO_2 (‰ versus V-PDB) and δ^{34}S of the total sulfur (‰ versus V-CDT) were determined at the Geological Institute (Moscow). Carbon isotopes were determined using a Finnigan Delta Plus XP continuous-flow IRMS coupled with a TRACE gas chromatograph system equipped with Porabond Plot capillary column (60 m., ID 0.32 mm) with accuracy 0.2‰. Sulfur isotopes were analyzed using a Delta V Advantage mass spectrometer equipped with the element analyzer Flash EA with accuracy 0.5‰.

Headspace gas from Giggenbach flasks and dry gas were analyzed in the INGV-Palermo for ^{3}He/^{4}He, ^{40}Ar/^{36}Ar, and ^{4}He/^{20}Ne ratios using a Helix SFT-CVI mass spectrometer following the procedure described in Rizzo et al. (2015). The ^{3}He/^{4}He values were corrected for air contamination using the ^{4}He/^{20}Ne ratios (Sano & Wakita, 1985) and expressed as R/R_A where R is the measured and R_A is the air ratio (1.39×10^{-6}; Mamyrin et al., 1970).

3.2. MultiGas Measurements

Simultaneously with the gas sampling from fumaroles into Giggenbach bottles, the measurements of plume composition were made with portable MultiGas analyzers. The analyzer used in 2016 was built in the INGV (Palermo) and was equipped with a Gas-Card NG CO_2 sensor with a 0–3,000 ppmV range, a City Tech SO_2 and H_2S sensors with 0–100 and 0–200 ppmm (mass) ranges, respectively, H_2 sensor with a 0–200 ppmm range. The set also included a relative humidity and pressure/temperature sensors. All detectors have been calibrated with certified standards. A 0.45 μm filter was attached at the entrance of gas driven by a membrane pump Boxer Series S. The analyzer used in 2017 was a home-built and lightweight multigas analyzer (Shinohara, 2005) composed of a Gas-Card NG CO_2 sensor with a 0–1,000 ppm range, a City Tech SO_2 sensor with a 0–50 ppm and City Tech H_2S sensor with a 0–20 ppm range. The data were registered every second by a MSR 145 data logger. Detection limit was around 4 ppm for the CO_2 sensor, 0.5 ppm for SO_2, and 0.3 ppm for H_2S. From the slopes of the best fit regression lines (with use the software "Ratiocalc v3"; Tamburello, 2015), we derive following characteristic molar ratios in the volcanic plume: CO_2/SO_2, SO_2/H_2S, and SO_2/H_2.

3.3. The SO_2 Flux

The SO_2 flux was measured by traversing below the plume with a zenith-pointing Ocean Optics USB 2000+ spectrometer recording the radiation of the diffuse sky radiance between 295 and 420 nm with a 0.5 nm

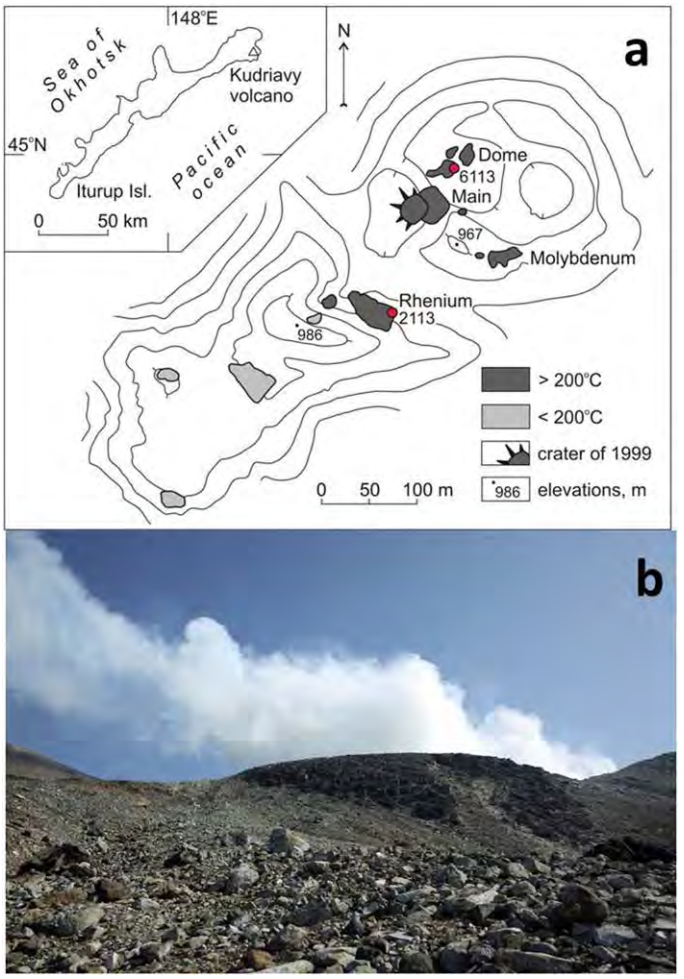

Figure 7. (a) Sketch map of the crater of Kudriavy volcano with the sampling points and (b) a typical plume from the Kudriavy crater in August 2017. Photo I. Chaplygin.

resolution. The spectra were processed with the Mobile DOAS program (Johansson et al., 2009). The fitting window was chosen to be 313–330, which is slightly longer wavelengths than the traditionally used by the NOVAC users. This spectral fitting window was chosen to cope with the low light intensity transmitted by the cloudy skies at these high latitudes, and also because, in most case, the walking traverses were made under proximal plumes with relatively high SO_2 column densities and aerosol contents (Fickel & Delgado Granados, 2017). Wind speeds used to calculate the flux were taken from the Global Data Assimilation System of the NOAA (https://www.ready.noaa.gov/READYamet.php) at the altitude of the considered volcanoes and by direct anemometer measurements.

4. Results and Discussion

4.1. Chemical and Isotopic Composition of Gases

4.1.1. Geochemistry of Major Components and C/S Ratio

Chemical composition of the gases is shown in Table 1. All gases are water-rich, and water content is practically independent on the vent temperature. Only for fumaroles of Pallas volcano the lower temperatures correspond (but not systematically) to some higher water content in the range of 939–986 mmol/mol. Gases from Sinarka, Kuntomintar, and Pallas volcanoes are relatively high in HCl, even in some low-temperature fumaroles. Fumaroles at Ebeko field can be divided into three groups: (1) high-temperature Active Funnel with a HCl content typical for the arc high-temperature volcanic gases ~5 mmol/mol (e.g., Taran & Zelenski, 2014); (2) low-temperature vents (~100°C) with HCl > 1 mmol/mol; (3) low-temperature vents with low HCl, ≪1 mmol/mol. In Table 1 only three gas analyses of the Ebeko fumaroles are shown for vents from these three groups. High HCl concentrations in low-temperature fumaroles may be caused by at least two processes: (1) conductive cooling of the primary magmatic fluid and (2) steam separation from the ultra-acidic boiling brine beneath the fumarolic field. The first case is probably related to fumaroles of Sinarka and Pallas volcanoes and is similar to low-temperature fumaroles of Satsuma Iwojima volcano, Japan (Shinohara et al., 1993). The second case can be observed at Poas (Costa Rica) and White Island (New Zealand) volcanoes (Christenson et al., 2017; Fischer et al., 2015; Giggenbach et al., 2003; Taran & Zelenski, 2014).

The ternary plots in Figures 8a and 8b show relative CO_2, S_{tot}, HCl, and HF concentrations, where $S_{tot} = SO_2 + H_2S$. For the comparison, the composition of the 1,060°C gases collected from a hornito above the lava flow during the Tolbachik-2013 eruption is plotted (Zelenski et al., 2014). The main feature of the Kurilian gases is low to very low molar C/S ratio (<1) even in low-temperature fumaroles (Figure 8b). This is characteristic for all but Kuntomintar volcano where C/S > 1 (2–5). Results for both direct sampling and MultiGas measurements give similar C/S values except Ebeko and Berg volcanoes where fumarolic plumes from high-temperature and low-temperature fields are separated (Table 1). The estimated average composition of gases those concentrations were measured by MultiGas in fumarolic plumes of Sinarka, Kuntomintar, and Pallas are also shown in Table 1 (normalized to the sum of H_2O, CO_2, H_2, H_2S, and SO_2). These concentrations generally differ from those determined analytically for the direct samples. Lower water content in fumarolic plumes is caused by partial condensation of fumarolic vapor, which leads to the apparent increase of the concentrations of other species in plumes. However, there is a good agreement in the C/S ratios between direct samples and plume gases. This can be seen in Figure 9 where both the C/S results from direct sampling and MultiGas measurements are shown.

Relative concentrations of CO_2, HCl, and HF are plotted on a ternary plot in Figure 8a. It can be seen that most samples from Pallas and Sinarka volcanoes plot within a cluster together with magmatic gases of

Table 1
Chemical Composition of Volcanic Gases (mmol/mol) and Important Ratios

Sample	T (°C)	H_2O	H_2	CO_2	CO	SO_2	H_2S	HCl	HF	N_2	Ar	He	CH_4	C/S	S/Cl	N_2/Ar
Ebeko, Paramushir: 50°41′29″N; 156°01′01″																
F1	420	936.6	0.255	27.9	0.000033	23.9	5.74	5.64		0.18	0.00210	0.00012	0.000010	0.94	5.3	86
F6	102	898.5	0.00009	93.7	0.00001	1.20	2.22	3.8		0.51	0.00078	0.00063		28	0.9	637
F19	110	937.8	0.00002	61.2		0.63		0.04		0.49	0.00038	0.00081	0.00022	97	16	1,290
MultiGas	(*)													1.3		
MultiGas	(**)	974.7	0.0122	23.6		1.48	0.22							14		
Sinarka, Shiashkotan: 48°52′24″N; 154°10′54″E																
39m	440	975.9	0.222	6.13	0.00052	13.51		3.21	0.22	1.01	0.0093	0.000021	0.000049	0.45	4.2	108
10i	315	977.6	0.110	8.50	0.00003	15.15	3.09	2.71	0.19	0.36	0.0034	0.000063	0.000020	0.47	6.7	106
17m	215	982.8	0.063	5.50	0.00013	8.11		3.40	0.18	0.10	0.0003	0.000001	0.000011	0.68	2.4	333
MultiGas		963	0.6	12		12	16							0.43		
Kuntomintar, Shiashkotan: 48°45′28″N; 154°00′54″E																
4m	260	979.4	0.016	15.6		3.56		1.15	0.08	0.25	0.0007	0.000066	0.000166	4.4	3.1	357
12i	250	975.5	0.021	16.0	0.00003	7.61		1.89	0.06	0.39	0.0009	0.000055	0.000260	2.1	4.0	433
16m	200	980.6	0.004	14.3		3.94		0.91	0.02	0.18	0.0006	0.000006	0.000260	3.6	4.3	300
12m	154	978.3	0.002	15.1		5.65		0.82	0.01	0.12	0.0002	0.000063	0.000006	2.7	6.9	600
15i	146	979.3	0.003	16.4	0.00002	2.60	0.79	0.63	0.04	0.24	0.0013	0.000059	0.000340	4.8	5.4	185
30i	130	974.5	0.005	16.6	0.00003	2.90	4.79	0.67	0.01	0.37	0.0013	0.000065	0.000030	2.2	11.5	284
MultiGas		940		35		9.4	14.5							1.6		
Pallas, Ketoy: 47°20′39″N; 152°28′47″E																
6i	722	964.7	3.03	5.62	0.0053	16.69	9.80	5.10	1.60	0.29	0.0090	0.000176	0.00017	0.21	5.2	32
2a	441	939.3	0.228	6.39	0.00015	48.31		4.63	0.91	0.08	0.0019	0.000068	0.000013	0.13	10.4	42
31m	286	955.7	0.034	7.83		27.32		6.80	1.17	2.46	0.0220	0.000043	0.000016	0.29	4.0	111
49m	227	945.6	0.004	2.38	0.000034	35.16	7.60	9.11		0.07	0.0006	0.000039	0.000000	0.06	4.7	117
14i	212	983.5	0.230	4.20	0.00057	4.43	6.15	1.33	0.06	0.09	0.0010	0.000123	0.000010	0.40	8.0	90
8a	122	952.1	0.153	5.57		22.02	9.77	7.25	0.53	0.31	0.0004	0.000065	0.000100	0.18	4.4	775
7i	103	983.1	0.143	4.97	0.0002	6.75	2.53	0.34	0.05	0.18	0.0009	0.000039	0.000030	0.54	27	200
19m	102	985.8	0.008	2.29		5.92	5.88	0.10		0.04	0.0004	0.000004	0.000004	0.19	120	100
MultiGas		945	1.4	8.0		32	16							0.17		
Kudryavy, Iturup: 45°22′57″N; 148°48′45″E																
KU6113	780	952.8	5.20	15.1	0.075		23.3	2.56	0.55	0.35	0.0097	0.00024	0.000004	0.65	9.1	36
KU2113	480	969.0	0.71	13.9	0.003		14.0	1.68	0.20	0.43	0.0049	0.00019	0.001203	0.99	8.3	87
Berg, Urup: 46°03′37″N; 150°03′56″E																
Be0117	96.8	968.7	0.15	28.5		1.58		0.17		1.59	0.0058	0.00013	0.0015	18	9.3	274
MultiGas	(E)												3.0			
MultiGas	(W)												1.3			

Note. All compositions are corrected for air extracting oxygen and corresponding N_2 and Ar concentrations. Also are shown the compositions estimated from the MultiGas analyses. MultiGas data for Ebeko volcano are for high-temperature (*) and low-temperature (**) fields. MultiGas data for Berg volcano are for the Eastern (E) and Western (W) craters. See text for more details.

Tolbachik and with a relatively high F content. In Kurilian samples, mole ratio Cl/F generally increases with decreasing temperature from ~3 for the highest-temperature fumarole of Pallas volcano to ~80 for fumaroles of Kuntomintar volcano.

Usually, concentrations of "acidic" species in volcanic gases (HCl, HF, and SO_2) under shallow conditions along cooling are controlled by so-called "scrubbing" or partial dissolution of these species in groundwater. Sulfur, additionally, can be lost from the uprising and cooling magmatic gas as native sulfur after oxidation of H_2S by the admixed air or air-saturated groundwater (Marini et al., 2011; Symonds et al., 2001; Taran et al., 1997a). Therefore, as a rule, low-temperature fumaroles have C/S ratio $\gg 1$ because CO_2 behaves as a conservative component, with a relatively low solubility in water, and thus reaches surface. This rule however is not valid for fumaroles of Sinarka, Kuntomintar, and Pallas volcanoes: the C/S ratio for these volcanoes does not depend on temperature. For example, the 720 and 102°C gases from the Pallas fumaroles (samples P1 and P8, Table 1) have the same C/S mole ratio of 0.2. Similar behavior is shown by gases from Sinarka and Kuntomintar fumaroles: the C/S values for Sinarka are all <1 and for Kuntomintar >1 (Figure 9). At Ebeko, only the high-temperature fumarole from the Active Funnel discharges gas with C/S <1. The C/S values for low-temperature fumaroles from other two groups (with high and low HCl, see above) are all $\gg 1$

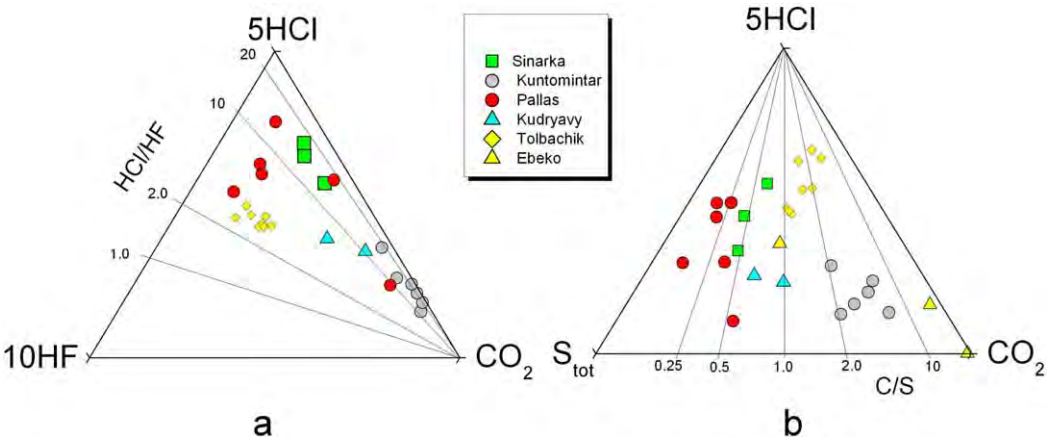

Figure 8. Relative concentrations of "acidic" components in fumarolic gases. (a) Ternary plot for relative concentrations of HCl, HF, and CO_2 and (b) the same for relative concentrations of HCl, CO_2, and S_{tot}. See text for more details.

indicating strong absorption and oxidation of S-species in the aquifer beneath the fumarolic field of Ebeko (Kalacheva et al., 2016).

Aiuppa et al. (2017) divided all arc volcanic gases into three groups (C/S < 2, 2 < C/S < 4, and C/S > 4) and attributed different C/S ratios to different contribution of CO_2 from different crustal/slab sources on a regional scale. However, in our case, drastically different C/S ratios are observed in fumaroles of two volcanoes on the same island with <20 km between their summits—Sinarka (C/S = 0.5 ± 0.1) and Kuntomintar (C/S = 3.1 ± 1) on Shiashkotan Island. The most probable reason for such a difference is a different degree of degassing of magma bodies beneath the fumarolic fields of both volcanoes. More degassed magma releases less CO_2 and becomes relatively enriched in more soluble volatiles (S, Cl, and F). Fluorine is the most soluble in silicate melts among analyzed species of volcanic gases (e.g., Aiuppa et al., 2002; Carroll & Webster, 1994; Dalou et al., 2015, and references therein). Therefore, the lower Cl/F ratios in Sinarka gases (16 ± 2) comparing to gases of Kuntomintar (42 ± 15, Figure 10) may relate to a much more degassed magma source for Sinarka volcano. The low ratios of C/S (~0.25) and Cl/F (~10) in the gases of Pallas volcano, Ketoy Island, may also indicate a significantly degassed magmatic source.

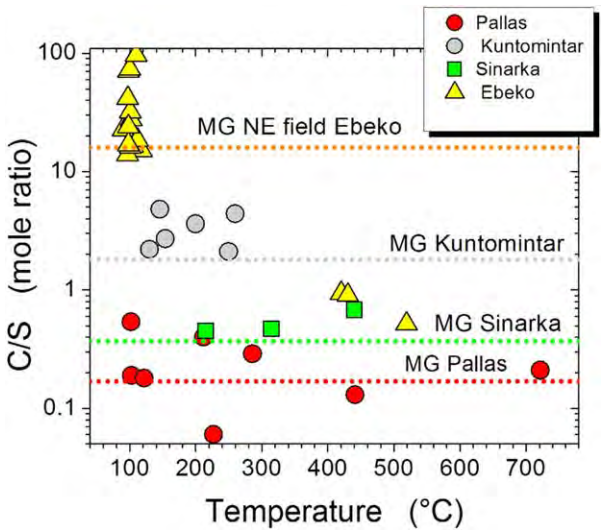

Figure 9. C/S ratios versus temperature of fumaroles. Dotted lines show the average C/S values measured by the MultiGas analyzer. More points for Ebeko are plotted using data from Kalacheva et al. (2016) and Menyailov et al. (1985).

Values of $R_H = \log(x_{H2}/x_{H2O})$ and $R_{CO} = \log(x_{CO}/x_{CO2})$ as functions of vent temperature for concentrations taken from Table 1 are shown in Figures 10a and 10b. The high-temperature points on both plots follow the trends for so-called "gas buffer" proposed by Giggenbach (1987) for equilibrium within the gas phase at 1 atm of the total pressure:

$$SO_2 + 3H_2 = H_2S + 2H_2O \quad (1)$$

In this case $R_H = 1.22 - 3581/T$ and $R_{CO} = 3.61 - 5829/T$ using thermodynamic data from Giggenbach (1987). On the R_{CO} and R_H versus 1,000/T (K) plots (Figures 10a and 10b) lines for so-called "rock buffer" are also shown, which corresponds to equilibrium of water vapor and CO_2 with a generalized mineral assemblage containing Fe(II)-bearing and Fe(III)-bearing minerals that is modeled by the H_2O-hematite-fayalite system (Giggenbach, 1987). Only points for high-temperature samples lie close to the gas buffer lines on both plots. The lower temperature fumaroles show compositions that most probably reflect partially quenched higher-temperature states not reequilibrated under lower temperature surface conditions.

All gases contain methane in low concentrations with an average CH_4/CO_2 ratio of $\sim 10^{-5}$.

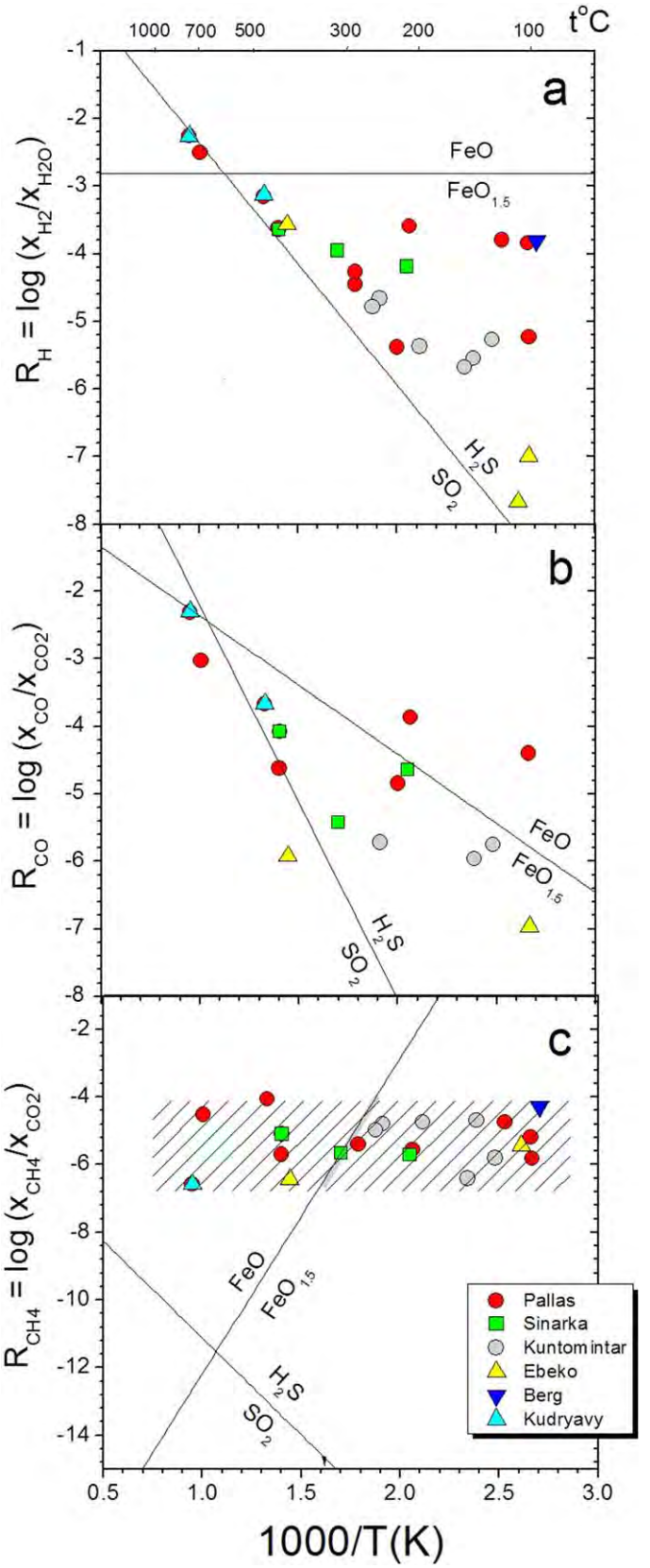

Figure 10. Redox diagrams for volcanic gases. (a) H_2/H_2O, (b) CO/CO_2, and (c) CH_4/CO_2. Theoretical (based on thermochemical data) buffer lines are also shown: FeO-$FeO_{1.5}$ is so-called "rock buffer" and H_2S-SO_2 is the "gas buffer" (Giggenbach, 1987). See text for discussion. Symbols as in Figure 8.

Table 2
Major and Trace Elements in the Highest-Temperature Condensates of Pallas Volcano

Volcano	Pallas	Pallas	Kudryavy	Rock, Pallas
T (°C)	720	656	590	
		ppb		ppm
Cl	14,209	13,597	1,140	
Ag	0.89	0.62	3.4	0.07
As	4,187	2,670	888	7
Au	2.29	0.68	0.49	0.05
B	40,009	44,060	7,104	25
Ba	117	125	101	152
Be	0.20	0.30	0.17	0.4
Bi	268	542	17	0.03
Br	19,054	16,346	1,848	4
Cd	209	1,874	87	0.1
Co	0.32	0.47	1.2	26
Cr	9.4	11.6	35	26
Cs	5.9	8.2	7.6	1
Cu	23	14	3.5	43
Ga	7.0	10.8	27	17
Ge	10.0	8.0	0.66	0.9
Hf	4.9	1.1	0.37	2.4
In	159	510	39	0.25
Li	567	448	489	6
Mo	27	16	13	1
Nb	0.56	0.13	0.11	1.7
Ni	32	18	102	5
Pb	450	430	357	4.5
Pd	0.07	0.04	0.053	0.02
Rb	36	42	8.3	13
Re	5.2	2.3	0.07	0.001
Sb	188	116	9.9	0.4
Sc	0.10	0.05	1.4	34
Se	1,852	1,278	117	0.9
Sn	3,345	1,595	55	0.8
Sr	116	138	126	288
Ta	2.3	0.59	0.40	0.1
Te	21	12	23	0.01
Th	0.30	0.12	0.20	1.1
Tl	125	491	25	0.1
U	0.04	0.06	0.01	0.44
V	0.77	1.01	11	274
W	0.16	0.05	0.27	1.0
Y	0.50	0.53	1.3	24
Zn	66	97	673	61
Zr	64	60	44	84
REE				
La	0.56	0.59	0.28	5.5
Ce	1.17	1.27	0.37	14.8
Pr	0.04	0.07	0.014	2.14
Nd	0.35	0.43	0.35	10.4
Sm	0.06	0.05	0.12	3.18
Eu	0.022	0.015	0.04	0.90
Gd	0.086	0.055	0.16	3.89
Tb	0.01	0.01	0.009	0.62
Dy	0.03	0.03	0.02	4.32
Ho	0.01	0.01	0.01	0.89
Er	0.03	0.04	0.03	2.83
Tm	0.004	0.004	0.002	0.41
Yb	0.061	0.052	0.029	2.74
Lu	0.022	0.017	0.01	0.39

Table 2. (continued)

Volcano	Pallas	Pallas	Kudryavy	Rock, Pallas
Major rock-forming elements				wt %
Si	129,496	171,298	25,290	26.6
Ti	63	420	345	0.46
Al	3,159	3,758	3,613	9.3
Fe	954	1,061	6,612	6.1
Mn	15	17	42	0.13
Mg	962	820	1,418	2.1
Ca	7,200	5,400	13,199	5.4
Na	15,501	20,909	2,797	2.4
K	10,551	14,019	3,584	0.9
P	23	8	56	0.06

Note. Composition of the Pallas andesite from this work.

As it is shown in Figure 10c, if the redox-state is controlled by the "rock" buffer, methane is close to equilibrium with CO_2 at temperatures in the range of 250–350°C independently on the vent temperature. This follows from the intersection range of the main trend with the FeO-$FeO_{1.5}$ buffer line (Figure 10c). For fumaroles with the outlet temperatures <300°C it could be explained as the attainment of equilibrium at a higher temperature but for the hotter fumaroles CH_4 and CO_2 apparently are in equilibrium with altered wall rocks at lower temperature, which does not make sense. In other words, methane in fumarolic gas of the studied volcanoes is not in equilibrium with CO_2 at any redox-buffering.

4.1.2. Trace Elements in Volcanic Gas Condensates

Concentrations of trace elements in condensates of the two high-temperature fumaroles of the Pallas volcano (720 and 656°C) and in the condensate from a fumarole of the Kudryavy volcano (780°C) sampled in August 2016 are shown in Table 2. In terms of enrichment factors normalized to Mg: $EF_i = (E_i/Mg)_g/(E_i/Mg)_r$, where E_i is concentration of element i and subscripts g and r stand for gas and rock, respectively (Figure 11), the patterns of trace elements in Pallas and Kudryavy condensates do not differ significantly. The general trend is similar to that for other high-temperature volcanic gas condensates reported in a number of studies (e.g., Momotombo, Quisefit et al., 1989; Kudryavy, Taran et al., 1995; Wahrenberger et al., 2002; Colima, Taran et al., 2001; Tolbachik, Zelenski et al., 2014).

For fluids separated from a common magmatic melt at temperatures >700°C, the concentrations of many important trace elements are controlled mainly by the stability of the gaseous species under redox-state of the fluid phase (Symonds & Reed, 1993; Taran et al., 2001; Wahrenberger et al., 2002). For the lower temperature condensates, most of the elements are precipitated on the fumarolic conduit walls along a temperature gradient, and only a portion may reach the surface in form of aerosols. Zelenski et al. (2014) discussed in detail how to discriminate contributions from the aerosol particles to the composition of the condensates consisting mainly of the rock dust and minerals condensed from gaseous species in the fumarolic conduit upon cooling. In some cases, reported for other high-temperature condensates enhanced abundances of specific elements may reflect either some features of the parent magmas or specific redox conditions. For example, the Tolbachik gases have transported relatively high amounts of Au (up to 8 ppb) and Cu (up to 20 ppm), which was interpreted as related to the specific magma composition (Zelenski et al., 2016). Enrichment in vanadium for high-temperature gases (to 820°C) from Colima (Mexico) was attributed to the high oxidation of the gas due to high air contamination and a high volatility of some of the oxidized V-species (Taran et al., 2001). Detailed analysis of the data on trace elements in condensates presented here is beyond the scope of this study. The last note to the discussion is related to the concentrations of rock-forming elements. Correlation between the concentrations of the rock-forming elements

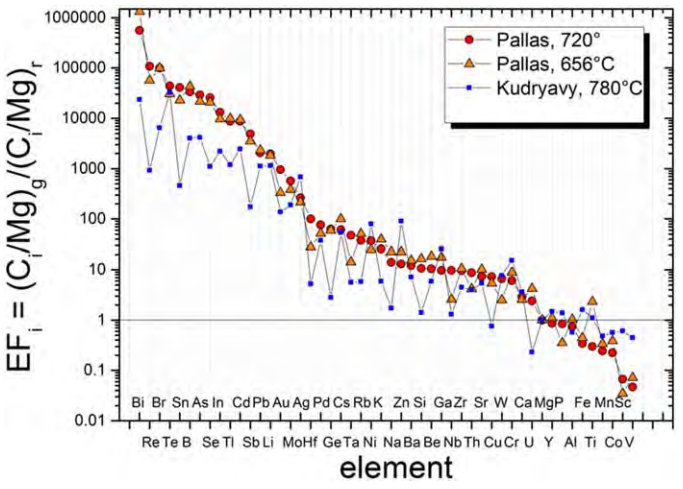

Figure 11. Enrichment factors (EF) normalized to Mg for two high-temperature volcanic gas condensates from Pallas volcano and a 780°C condensate from Kudryavy volcano. EF sorted by descending for the 720°C condensate of Pallas.

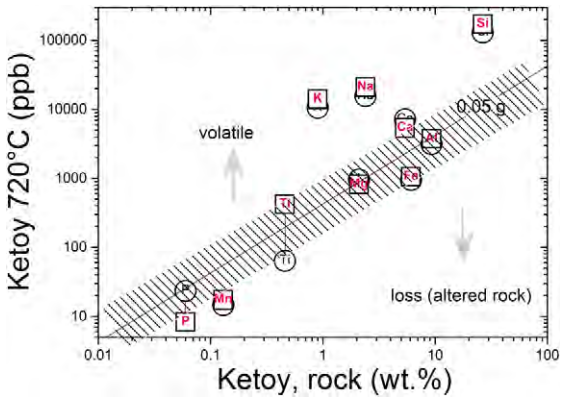

Figure 12. Correlation between rock and condensate compositions for rock-forming elements. See text for discussion.

in condensates and the composition of the potential host rock (andesite of the Pallas cone, Gorshkov, 1970) is shown in Figure 12, where the composition of two condensates from the Pallas volcano is presented. The correlation is generally good and corresponds to approximately 0.05 g of the dispersed rock aerosol per 1 kg of condensate, but Na, K, and Si are outside the main trend. For Na and K, this can be explained by their high volatility in form of chlorides. The high concentration of Si may have two main sources: (1) the contribution of the SiO_2-enriched aerosol from the highly altered wall rock and (2) leaching from the sampling glass (quartz) devices due to the high HF concentration in the condensate. The volatility of Si is limited to the stability of gaseous SiF_4, which decreases with increasing temperature and cannot account for such high concentrations (e.g., Symonds & Reed, 1993). In turn, the lower concentrations of rock-forming elements can be caused by the presence of dust of altered rock from the conduit walls and individual mineral particles.

4.1.3. Systematics of the N_2-Ar-He-Ne Composition

Almost all samples from fumaroles of Kuril volcanoes demonstrate significantly higher ratios of N_2/Ar than the air ratio of 84, indicating the presence of the nonatmospheric nitrogen. The maximum of 1,290 was analyzed in a low-temperature fumarole of the Ebeko volcano (Table 1). Data for all samples are plotted in Figure 13a on the ternary N_2-Ar-He diagram (Giggenbach, 1991). The diagram in Figure 13b demonstrate that ratios Ar/Ne in all gases fall between values for air and air-saturated water (ASW) indicating that Ar and Ne are generally "contaminates": their very high concentrations in air and ASW make impossible to estimate their magmatic abundances from the gas chemistry.

4.1.4. Helium and Carbon Isotopes, $C/^3He$ and $N_2/^3He$

An average value of $5.4R_A$ has been estimated for arc fluids by Hilton et al. (2002) based on a data set available at that time, which includes many low $^3He/^4He$ ratios for geothermal gases. Later, Sano and Fischer (2013) raised this estimate up to $7R_A$ based on an updated data set. The most representative arc fluids are either discharged by arc volcanoes as volcanic gases or stored in the melt inclusions in olivines of the erupted rocks. Our data show that volcanic gases of Kuril Islands contain He with the MORB-type helium. The along-arc distribution of the $^3He/^4He$ values is uniform from the northern Ebeko volcano on Paramushir Island until Kudriavy volcano on the southern Iturup Island: Maximum of $7.7R_A$ is measured in the Active Funnel of Ebeko volcano on Paramushir Island, $7.6R_A$ in gases of Kuntomintar, Shiashkotan Island, up to $8.3R_A$ in fumaroles of Pallas, Ketoy Island, and $7.7R_A$ in fumaroles of Kudryavy, Iturup Island (Table 3). Taran et al. (1993, 2009) reported a value of $7.3R_A$ in steam vents of the Ushishir volcano, the next island to the north of Ketoy. However, Kalacheva et al. (2017a, 2017b) reported low $^3He/^4He$ values for gases from two southernmost volcanoes of the Kuril chain, Mendeleev, and Golovnin, both on Kunashir Island. These values, $(5.4 \pm 0.2)R_A$ for Mendeleev (six samples) and $(3.4 \pm 0.2)R_A$ for Golovnin (six samples), are much lower than the MORB-like ratios in gases of all degassing volcanoes of the Kuril arc. All the

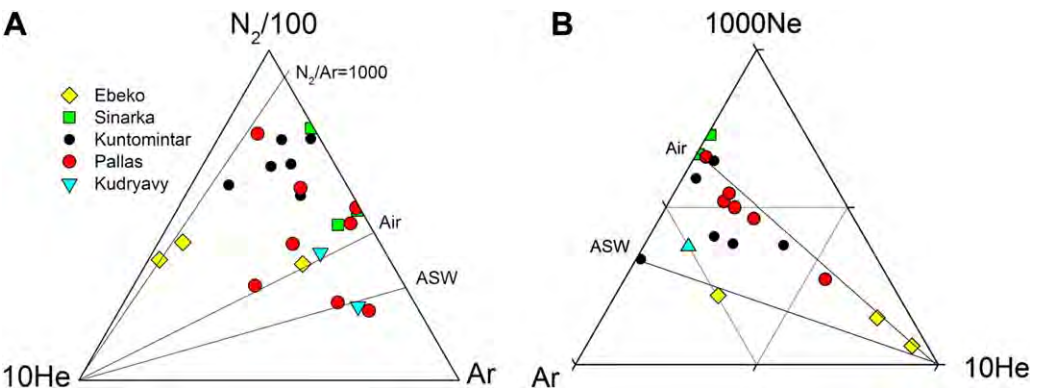

Figure 13. Relative concentrations of N_2 and noble gases (He, Ne, and Ar) in the Kuril volcanic gases. (a) N_2-Ar-He and (b) He-Ar-Ne.

Table 3
Isotopic Composition of Fumarolic Gases

Sample	T (°C)	δD	δ^{18}O	δ^{13}C-CO_2	δ^{34}S - Stot	^{3}He/^{4}He corr	^{4}He/^{20}Ne	^{40}Ar/^{36}Ar	$CO_2/^3$He ($\times10^{-9}$)	$N_2/^3$He ($\times10^{-8}$)
Ebeko, Paramushir										
F1	420	−24.6	2.57	−4.3		7.90	129	295	21	1.4
F6	104	−45.6	−2.30	−2.2		7.83	510	314	13.4	0.75
F19	101	−49.7	−5.55	−3.4		7.63	1,506	310	6.7	0.53
Sinarka, Shiashkotan										
39m	440	−21.3	5.7		2.5	6.8	1.1	293	3.1	
10i	315	−22.0	4.2		2.0					
17m	215	−23.4	4.4	−1.3	1.6	5.4	1.2	295	73.3	99.9
Kuntomintar, Shiashkotan										
4m	260	−25.3	4.1	−2.0	0.0	7.5	56	309	22.7	2.8
12i	250	−23.0	2.7		2.4	7.5	38	305	5.9	1.1
16m	200	−27.1	2.3	−2.6	6.7	6.1	4.7	299	6.5	0.59
12m	154	−29.7	1.5	−2.0	4.5	7.6	204	313	238	15.8
15i	146	−38.3	0.5	−2.2	5.0	7.3	29	301	4.8	0.38
30i	130	−21.2	4.5		9.5	7.7	28	304	51.7	8.1
Pallas, Ketoy										
6i	722	−21.1	5.8	−4.2	3.5	7.0	9.1	296	3.3	
2a	441	−25.3	5.9		2.2					
31m	286			−5.2	3.5	7.8	3.8	302	16.8	13.1
49m	227	−25.0	6.1	−4.5	4.7	8.3	63	299	5.3	0.45
14i	212	−43.6	−1.7	−4.1	6.9					
8a	122				4.6	8.1	101	300	7.6	3.8
7i	103	−41.9	−0.1		7.5	7.0	44	302	13.1	2.9
19m	102	−34.0	1.7		10.3	8.3	6.3	297	49.6	1.5
Berg, Urup										
5i	96.8					7.9	188	306	19.7	11
Kudryavy, Iturup										
KU6113	780	−21	6.3			7.73	33.0		26	1.4
KU2113	480	−41.6	−0.83						87	

Note. ^{3}He/^{4}He in R/R_A where R, measured ratio and R_A, air ratio of 1.4×10^{-6}. δD and δ^{18}O relative to V-SMOW; δ^{13}C relative to V-PDB and δ^{34}S relative to V-CDT.

compositions of fumarolic gases with known ^{3}He/^{4}He, $CO_2/^3$He, and δ^{13}C-CO_2 (Table 3, and data from Kalacheva et al., 2017a, 2017b) are plotted in Figures 14a and 14b following Sano and Marty (1995). Carbon isotopic composition of fumarolic CO_2 varies from ~–5‰, which is close to the MORB average value (e.g., Bottinga & Javoy, 1989), to heavier values up to −1.3‰ in Sinarka fumaroles. Trends on both plots are thus directed from the mantle to marine carbonate values. Taking into account that pelagic sediments in this sector of the NW Pacific are poor in carbonates (e.g., Bailey, 1996; Jarrard, 2003) is inferred that carbonates in altered oceanic crust are a significant source of CO_2. The $N_2/^3$He versus ^{3}He/^{4}He plot shown in Figure 15 partially confirms the contribution of volatiles from the AOC especially, for the southern Kunashir Island. The mixing lines here are taken from Taran (2011).

High ^{3}He/^{4}He values in gases of the Kuril arc are consistent with the close to MORB values of ^{87}Sr/^{86}Sr in volcanic rocks (0.7028–0.7031) along the arc (Avdeiko et al.,2002; Martynov et al., 2010, among others). In turn, the lower ^{3}He/^{4}He values in Kunashir gases are consistent with the higher values of ^{87}Sr/^{86}Sr, up to 0.7048, reported for Miocene basalts and basaltic andesites of the Kunashir Island (Martynov, 2013) and indicating more complex structure of the southern segment of the Kuril subduction zone with involving some recycled, accreted or underlying crustal material.

4.1.5. Water Isotopes

Isotopic compositions of the volcanic gas condensates (Table 3) show a typical "arc" trend from meteoric water line to the "Andesitic" or "Arc water" composition (AW; Giggenbach, 1992; Taran et al., 1989) as it can be seen in Figures 16a–16c. Some of the data for Ebeko fumaroles are taken from other sources (Kalacheva et al., 2016; Menyailov et al., 1985). Points for low-temperature fumaroles of Ebeko on the δD versus δ^{18}O plot (Figure 16a) lie on the same trend but form a separate group on both plots where the dependence of

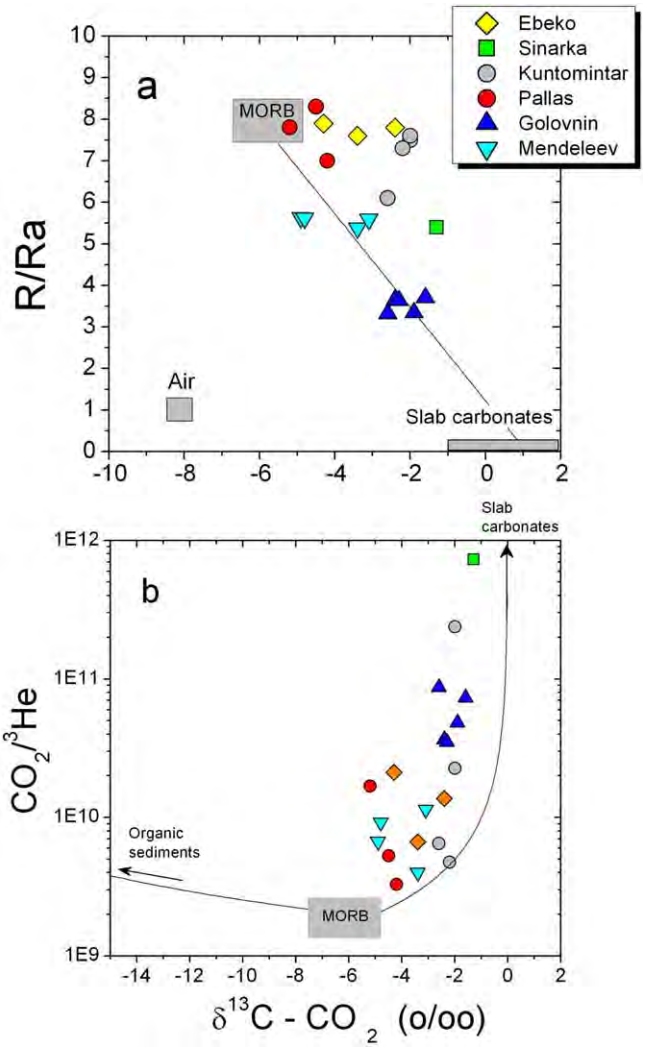

Figure 14. $CO_2/^3He$-$^3He/^4He$-$\delta^{13}C(CO_2)$ diagrams for the Kurilian volcanic gases with addition of the data from Kalacheva et al. (2017a, 2017b) for volcanoes of Kunashir Island. See text for discussion.

δD and $\delta^{18}O$ on the chloride content is shown (Figures 16b and 16c). The reason for such a high chloride content and relatively isotopically light water in the low-temperature fumarolic gas of Ebeko have been discussed in Kalacheva et al. (2016). It occurs because the southern and the SE fumarolic fields of Ebeko discharge vapor derived from boiling of shallow brine composed of the volcanic gas condensate and meteoric water. Note that the high-temperature Ebeko fumarole in the Active Funnel (420°C) has the HCl content and the isotopic composition of vapor in a typical range for the arc volcanic gases (e.g., Taran & Zelenski, 2014).

4.1.6. Sulfur Isotopes

The isotopic composition of the total fumarolic sulfur ($SO_2 + H_2S$) is shown in Table 3. It varies between 0‰ and +10‰, and in the highest-temperature (722°C) fumarole of the Pallas volcano $\delta^{34}S = +3.2‰$. The general trend shows isotopically heavier sulfur in the lower temperature fumaroles (Figure 17). According to Taylor (1986), Marini et al. (2011), and Kagoshima et al. (2015), the arc volcanic sulfur is characterized by large variations in $\delta^{34}S$ values but generally with positive $\delta^{34}S$ in a range of 0‰ to +14‰ indicating the contribution to sulfur of arc volcanoes from at least three sources: the upper mantle, oceanic sediments, and altered oceanic crust. In the last compilation of the sulfur isotope data for high-temperature volcanic gases that includes a very light value of −8.9‰ from Galeras volcano (Colombia) and a very heavy ratio of +11.7‰ from Satsuma Iwojima volcano (Japan), Kagoshima et al. (2015) determined an average value for $\delta^{34}S$ to be +4.6‰. Two large data sets from arc volcano islands, Vulcano (Cortecci et al., 1996) and White Island (Rafter et al., 1958), revealed the average $\delta^{34}S$ value for the total fumarolic sulfur of both volcanoes close to +3‰. The isotopic composition of the total sulfur from a 770°C fumarole of Kudryavy is +2.9‰ (Taran et al., 1995). The values of $\delta^{34}S$ in the 700–800°C gas of Colima (Mexico) are between +2.9‰ and +3.8‰ (Taran et al., 2001). Sulfur releasing from magma, has quite variable isotopic composition at the surface due to multiple redox-species and relatively fast isotopic exchange between species at high temperature. Below ~440°C, the boiling point of elemental sulfur, a part of the volcanic sulfur precipitates from the gas as the sulfur melt, and below 114–119°C as solid rhombic sulfur. Elemental sulfur is isotopically lighter than SO_2: the isotopic fractionation between SO_2 and solid S is poorly known but seems to be close to that between SO_2 and H_2S (Grinenko & Thode, 1970). Therefore, the most representative isotopic composition of the arc magmatic sulfur would be the total sulfur of high-temperature (>440°C) volcanic gases. Marini et al. (2011) explained the variability of the sulfur isotopic composition of fumarolic gases as a consequence of the variations in H_2S/SO_2, hydrolysis of native sulfur, loss of sulfur as sulfate dissolved in meteoric waters. The two trends shown in Figure 17 can be caused by two different processes: (i) a loss (precipitation) of the isotopically lighter native sulfur at low temperatures and a corresponding isotopic fractionation, which can be controlled by reaction:

$$SO_2(g) + 2H_2S(g) = 3S\downarrow + 2H_2O(g) \quad (2)$$

and (ii) recombination of SO_2 in the liquid phase with the dissolved isotopically heavier sulfate left in the acidic brine beneath a fumarolic field:

$$4SO_2(g) + 4H_2O = 3H^+ + 3HSO_4^- + H_2S(a) \quad (3)$$

Therefore, the isotopic composition of the total sulfur in low-temperature fumaroles can be used as an indicator of the presence of the acid volcano-hydrothermal system (if $\delta^{34}S < 3‰$).

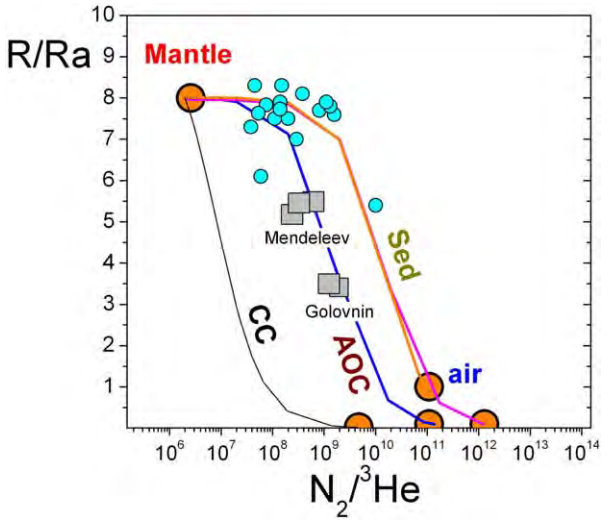

Figure 15. Helium isotopic composition versus $N_2/^3He$ for volcanic gases of Kuril Islands. Blue circles are data from this work and gray squares are from Kalacheva et al. (2017a, 2017b). Mixing lines are from Taran (2011).

4.2. The SO_2 Flux

Before 2015, the SO_2 flux within the Kuril arc has been measured only once in 1995 by Fischer et al. (1998) using COSPEC on Kudryavy volcano. It was reported to be between 75 and 100 t/d. Taran (2009) estimated the total SO_2 flux from passively degassing volcanoes of the Kurilian arc to be ~1,000 t/d comparing heights of the fumarolic vapor plumes. During 2015–2017, we succeeded in measuring fluxes from six volcanoes of the arc: Ebeko (Paramushir), Chirinkotan, Kuntomintar (Shiashkotan), Pallas (Ketoy), Berg (Urup), and Kudryavy (Iturup). All data on the SO_2 flux and the calculated fluxes of CO_2, H_2S, and HCl are compiled in Table 4.

4.2.1. Ebeko Volcano, Paramushir Island

Three attempts have been made at Ebeko in August 2015 before the beginning of a new period of phreatic activity that started 2 months later. The fumarole in the Active Funnel with temperature of 420–510°C produced up to 120 m high steam plume when the wind velocity was less than 3–4 m/s (Figure 2). Measurements made on 12, 13, and 15 August under different wind conditions at the distance about 1 km from the plume resulted, respectively, in 95 ± 30 t/d, 85 ± 25 t/s, and 104 ± 18 t/s. The next measurement was performed on 18 July 2017, from a boat about 15 km from the volcano, down to the wind. According to the GDAS model, the wind speed at that time and altitude was 9 m/s. and this measurement gave 210 ± 25 t/d of the SO_2 flux. Two walking traverses were made under the plume in 14 August 2017 with the wind speed taken by the handheld anemometer. The SO_2 fluxes calculated from these traverses are 280 ± 30 and 210 ± 30 t/d. Considering the high SO_2 column density and aerosol content of this proximal plume, it is possible that these values represent lower estimates of what is actually emitted by the active vent.

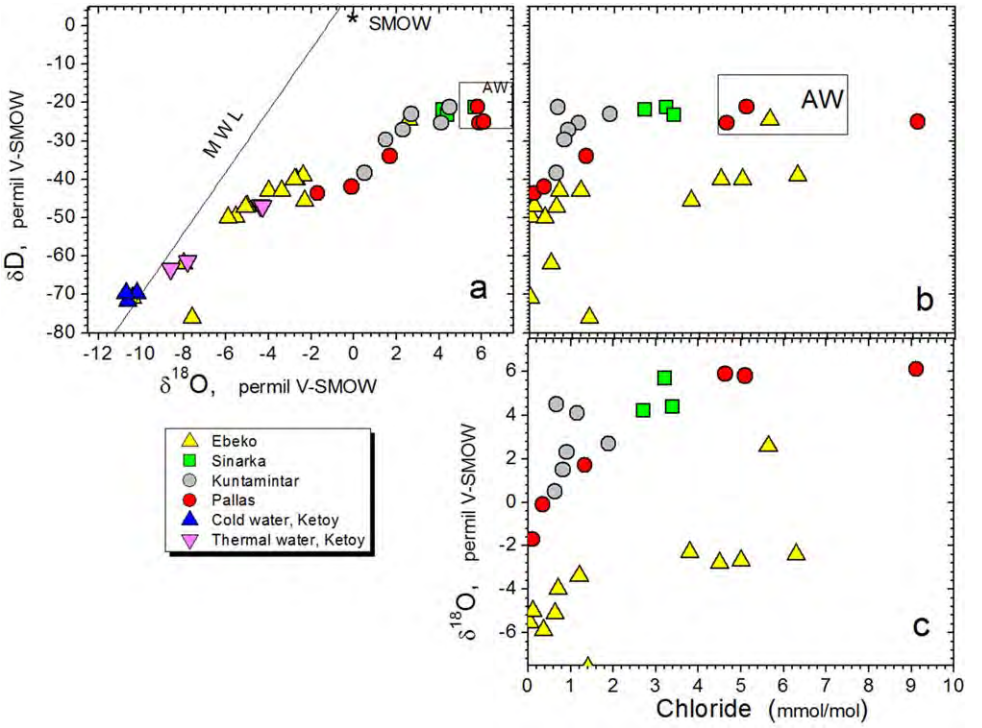

Figure 16. Isotopic composition of the volcanic gas condensate and chlorine content. (a) δD versus $\delta^{18}O$ plot for all sampled condensates and meteoric waters (Table 3) and (b, c) δD and $\delta^{18}O$ versus chlorine content. MWL, Meteoric Water Line; AW, "Andesitic" (Arc) Water (Taran et al., 1989).

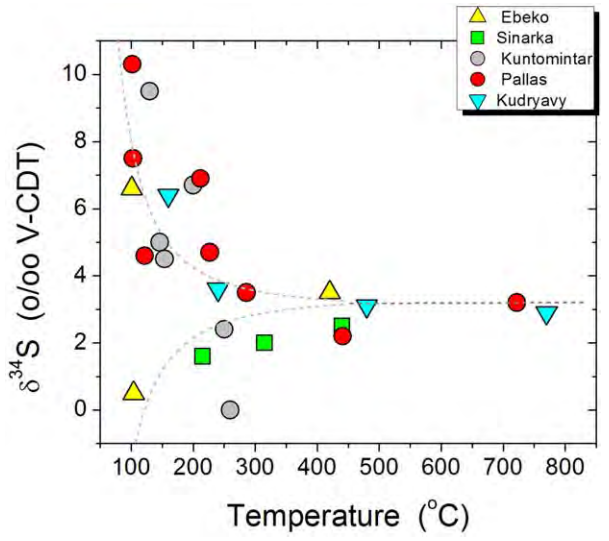

Figure 17. Sulfur isotopic composition of the total sulfur ($SO_2 + H_2S$) versus temperature of fumarolic vents. Dashed lines are two main trends that can be indicators either native sulfur precipitation or the presence of acid brine beneath fmaroles. See text for discussion.

4.2.2. Kuntomintar Volcano, Shiashkotan Island

The measurements were performed in 2016 on 26 July using ScanDOAS system from a fixed position approximately 900 m from the crater. The wind speed measured by the handheld anemometer was 8–10 m/s, and the plume was close to the relief. The maximal recorded flux during 2 h of measurements was 99 ± 25 t/d with the maximal SO_2 concentration of 170 ppmm (mass).

4.2.3. Chirinkotan Volcano-Island

On 12 August 2017, DOAS measurements were performed by traversing under the plume by the boat. Weather was cloudy and neither the plume nor the top of the volcano were visible. Nevertheless the plume was clearly detected with the DOAS during two successful traverses. The first traverse yielded a SO_2 flux of 230 t/d and the second 270 t/d. These values place Chirinkotan within the strong gas emitters of the Kuril Island, so a future campaign to measure the plume composition for this volcano would be useful in order to complete the volatile inventory of the archipelago.

4.2.4. Pallas Volcano, Ketoy Island

On 24 July 2016, ScanDOAS measurements were performed from a fixed position ~500 m from the fumarolic field of the Pallas volcano. The weather conditions were comfortable, with a clear sky and the wind speed of 4.5–5 m/s measured by anemometer. The average SO_2 flux was calculated to be 475 ± 30 t/d with a maximum of 750 t/d and maximum concentration of 1,800 ppmm.

4.2.5. Berg Volcano, Urup Island

Three walking traverses were performed from the flat southern floor of the Berg caldera on 6 August 2017. On two traverses the profile of the SO_2 column density showed two distinct maxima ascribed to the plumes of the two craters (Figure 5c). The three traverses resulted in the following SO_2 fluxes: 200, 290, and 230 t/d with an average of 240 ± 50 t/d. From the bimodal SO_2 concentration of the plumes, it was possible to estimate the fluxes from two craters as separately ~200 and ~40 t/d, respectively.

4.2.6. Kudryavy Volcano, Iturup Island

Two walking traverses were made on Kudryavy in 2016: 15 October and 19 October. Both were performed under the plume at the distance near 1 km from the source and resulted in close values of 360 and 330 t/d, which is much higher than the flux of 75–100 t/d measured in 1995 by Fischer et al. (1998). On August–September 2017, several walking traverses were made under the plume with the resulting flux of 370 ± 45 t/d. Changes in the activity of Kudryavy have started in 1999 when a phreatic explosion formed a small pit crater between high-temperature and low-temperature fumarolic fields (Chaplygin et al., 2016). Now a clear increase in the gas activity and a redistribution of temperatures and vents within the high-temperature

Table 4
Gas Fluxes From Volcanoes of the Kuril Arc in 2015–2017 (t/d)

Volcano	Location	Date	SO_2 flux	CO_2 flux	H_2S flux	HCl flux	SO2 flux, OMI[a]
Ebeko	N 46°06′, E 150°07′	12–15 Aug 2015	**100 ± 20**				
Ebeko	N 46°06′, E 150°07′	18 Jul, 14 Aug 2017	250 ± 30	160 ± 100	74 ± 30	46 ± 15	496[b]
Kuntomintar	N 48°45′, E 154°01′	18 Jul 2016	100 ± 30	220 ± 40	35 ± 10	17 ± 6	
Sinarka[a]	N 48°52′, E 154°10′	20 Jul 2016	≥100	≥40	≥60	≥20	
Chirinkotan	N 48°98′, E 153°48′	12 Aug 2017	250 ± 20				
Pallas	N 47°21′, E 152°29′	24 Jul 2016	480 ± 40	150 ± 20	80 ± 10	95 ± 10	140
Berg	N 50°41′, E 156°01′	6 Aug 2017	240 ± 50	843 ± 150	220 ± 70	25 ± 10	
Kudryavy	N 45°23′, E 148°49′	15 and 19 Oct 2016	**330 ± 60**				
Kudryavy	N 45°23′, E 148°49′	26, 29 Aug, 6, 29 Sep	370 ± 50	210 ± 40	110 ± 20	120 ± 20	187
Total		2016–2017	1,800 ± 300	≥1,250 ± 350	>500	>310	

Note. The SO_2 flux was measured by the mini-DOAS technique. Fluxes for other gases are estimated using MultiGas and average C/S weight ratios for the direct sampled high-temperature fumaroles (Table 1). The 2015 data for Ebeko and 2016 data for Kudryavy (bold entries) are not included in the total flux.
[a]The average SO_2 flux during the 2006–2016 decade measured from space according to Carn et al. (2017). [b]Ebeko + Chikurachki.

northern sector of the crater are observed. Fumarolic temperatures at the famous "Rhenium Field" increased from 400–500 to 600–700°C, which is accompanied with the disappearance of the surface incrustations of ReS_2 (Korzhinsky et al., 1994).

5. Summary and Comparison With Other Arcs

Volcanic gases from high-temperature fumaroles of the Kuril arc are similar to gases of other island arcs with generally >95 mol % of water vapor, and water and carbon isotopes close to the average arc magmatic values (Giggenbach, 1996; Shinohara, 2013; Taran, 2009; Taran & Zelenski, 2014). The Kuril island arc hosts many volcanoes with the permanent high-temperature fumaroles. Temperatures higher than 400°C were recorded at Ebeko (Paramushir), Sinarka (Shiashkotan), Pallas (Ketoy), and Kurdyavy (Iturup). High-temperature Kuril gases as a rule have the CO_2/S_{tot} mole ratios <1 and belong to the first group of the arc volcanic gases according to the classification by Aiuppa et al. (2017). All high-temperature and low-temperature volcanic gases of the Kuril arc are characterized by high $^3He/^4He$ values, between $7R_A$ and $8R_A$, with a maximum of $8.3R_A$ in gases of Pallas volcano (Ketoy Island) in the middle of the arc. Only the two southernmost volcanoes of the arc, Mendeleev and Golovnin on Kunashir Island emit gases with significantly lower $^3He/^4He$ of $5.5R_A$ and $3.3R_A$, respectively, indicating a significant contribution of He from the underlying crust. This is similar to the Lesser Antilles island arc where the southern part is characterized by much lower $^3He/^4He$ ratios and much higher $^{87}Sr/^{86}Sr$ values than the central part of the arc (measured in rock samples; Van Soest et al., 2002). The Kuril Trench is not accretionary except the southern Lesser Kuril Chain, which is parallel to Kunashir Island to the East, and this may be a reason for the crustal contamination of volcano-hydrothermal fluids of Kunashir (see also Kalacheva et al., 2017b). The carbon isotopic composition of volcanic CO_2 is on average is somewhat heavier than the MORB range of $-7‰$ to $-5‰$. The $^3He/^4He$-$\delta^{13}C$-$CO_2/^3He$ systematics of the Kurilian volcanic gases show mixing between the upper mantle CO_2 and (marine) carbonates or altered oceanic crust. The isotopic composition of the total sulfur in fumaroles with high temperatures approaches a value of $\sim+3‰$. This value is close to the isotopic composition of total sulfur in gases of arc volcanoes belonging to quite different arc settings like Vulcano, Italy; White Island, New Zealand; Colima, Mexico.

The global SO_2 flux from passively degassing volcanoes of subduction zones is estimated by different authors to be close to 50,000 t/d (Andres & Kasgnoc, 1998; Carn et al., 2017; Halmer et al., 2002). The distribution of the SO_2 flux over the active arcs is not uniform: for example, a relatively short Vanuatu arc (~1,200 km, similar to Kurilian arc) emits from ~8,000 t/d (Bani et al., 2012) to more than 12,000 t/d (Carn et al., 2017) of SO_2. The satellite data for Indonesia (~4,000 km long) reveal a flux of ~6,000 t/d (Carn et al., 2017). The SO_2 emission from volcanoes of the longest South America volcanic chain (~5,000 km) is estimated to be ~3,700 t/d (Carn et al., 2017). The gas emission from passively degassing volcanoes also significantly varies over time. For example, the measured SO_2 flux from the southern part of the Central American arc (SCAVA, volcanoes in Nicaragua and Costa-Rica) according to Andres and Kasgnoc (1998), Mather et al. (2006), and Aiuppa et al. (2014) was more or less constant, near 2,000 t/d, during the period of 1972 to 2014. However, de Moor et al. (2017) have measured the flux of ~6,000 t/d in 2015–2016, about 3 times higher. It should be noted that the SCAVA is almost 2 times shorter than the Kuril arc (~650 km versus ~1,200 km).

The total length of active subduction zones with the modern volcanism is ~40,000 km (Stern, 2002). It means that the normalized global SO_2 flux on average is ~1.25 t d^{-1} km^{-1}. According to our measurements, the Kuril arc passively emits at least 1,800 t/d of SO_2 or ~1.5 t d^{-1} km^{-1}. The measured SO_2 flux from the Kuril arc is thus ~2 times higher than it was estimated by Taran (2009).

Acknowledgments
This work was supported by a grant from the Russian Science Foundation 15–17-20011 and partially from the DECADE program of the Deep Carbon Observatory and a grant from the Richard Lounsbery Foundation for R.C. and R.K. Authors thanks the screws of "Afina," "Ashura," and "Larga" boats for their heroic assistance during our Kuril expeditions in 2016 and 2017. Many thanks to Andrea Rizzo for He and Ar isotope analyses and Katia Voloshina and Pavel Voronin for analytical help. We also thank the reviewers F. Tassi and J. M. de Moor for useful comments and suggestions. All data are in Tables (1–4).

References

Aiuppa, A., Federico, C., Paonita, A., Pecoraino, G., & Valenza, M. (2002). S, Cl and F degassing as an indicator of volcanic dynamics: The 2001 eruption of Mount Etna. *Geophysical Research Letters*, *29*(11), 1559. https://doi.org/10.1029/2002GL015032

Aiuppa, A., Fischer, T. P., Plank, T., Robidoux, P., & Di Napoli, R. (2017). Along-arc, inter-arc and arc-to-arc variations in volcanic gas CO_2/S_T ratios reveal dual source of carbon in arc volcanism. *Earth Science Reviews*, *168*, 24–47.

Aiuppa, A., Robidoux, P., Tamburello, G., Conde, V., Galle, B., Avard, G., et al. (2014). Gas measurements from the Costa Rica-Nicaragua volcanic segment suggest possible along-arc variations in volcanic gas chemistry. *Earth and Planetary Science Letters*, *407*, 134–147.

Andres, R. J., & Kasgnoc, A. D. (1998). A time-averaged inventory of subaerial volcanic sulfur emissions. *Journal of Geophysical Research*, *103*(D19), 25251–25261.

Avdeiko, G. P., Popruzhenko, S. V., & Palueva, A. A. (2002). The tectonic evolution and volcano-tectonic zonation of the Kuril-Kamchatka island-arc system. *Geotectonics*, *36*, 312–327.
Bailey, J. C. (1993). Geochemical history of sediments in the northwestern Pacific Ocean. *Geochemical Journal*, *27*(2), 71–91.
Bailey, J. C. (1996). Role of subducted sediments in the genesis of Kurile–Kamchatka island arc basalts: Sr isotopic and elemental evidence. *Geochemical Journal*, *30*(5), 289–321.
Bani, P., Oppenheimer, C., Allard, P., Shinohara, H., Tsanev, V., Carn, S., et al. (2012). First arc-scale volcanic SO_2 budget for the Vanuatu archipelago. *Journal of Volcanology and Geothermal Research*, *211–212*, 36–46. https://doi.org/10.1016/j.jvolgeores.2011.10.005
Botcharnikov, R. E., Knyazik, V. A., Steinberg, A. S., & Steinberg, G. S. (1998). Emission of gases, rock- and oreforming components on Kudriavy volcano, Iturup Isl., Kurile Islands. *Doklady Earth Sciences*, *361*, 858–861.
Botcharnikov, R. E., Shmulovich, K. I., Tkachenko, S. I., Korzhinskii, M., Rybin, A. V., & Shmulovich, K. I. (2003). Hydrogen isotope geochemistry and heat balance of a fumarolic system: Kudriavy volcano, Kuriles. *Journal of Volcanology and Geothermal Research*, *124*(1–2), 45–66.
Bottinga, Y., & Javoy, M. (1989). MORB degassing: Evolution of CO_2. *Earth and Planetary Science Letters*, *95*(3–4), 215–225.
Carn, S. A., Fioletov, V. E., McLinden, C. A., Li, C., & Krotkov, N. A. (2017). A decade of global volcanic SO_2 emissions measured from space. *Scientific Reports*, *7*, 44095. https://doi.org/10.1038/srep44095
Carroll, M. R., & Webster, J. D. (1994). Solubilities of sulfur, noble gases, nitrogen, chlorine and fluorine in magmas. *Reviews in Mineralogy and Geochemistry*, *30*, 231–279.
Chaplygin, I., Taran, Y., & Inguaggiato, S. (2016). *High-temperature fumarolic activity at Kudriavy volcano (Iturup Isl., Kuriles) during past 25 years*. Goldschmidt Conference Abstracts.
Chirkov, A. M., Barabanov, L. N., Basharina, L. A., & Zelenov, K. K. (1972). The activity of some volcanoes of the Kuril Islands in the summer 1970 [in Russian]. *Bulletin of Volcanological Stations*, *48*, 33–39.
Christenson, B. W., White, S., Britten, K., & Scott, B. J. (2017). Hydrological evolution and a chemical structure of a hyper-acid spring-lake system on Whakaari/White Island, NZ. *Journal of Volcanology and Geothermal Research*, *346*, 180–211.
Cortecci, G., Ferrara, G., & Dinelli, E. (1996). Isotopic time-variations and variety of sources for sulfur in fumaroles at Vulcano island, Aeolian archipelago, Italy. *Acta Vulcanologica*, *8*, 147–160.
Dalou, C., Le Losq, C., Mysen, R. O., & Cody, G. D. (2015). Solubility and solution mechanisms of chlorine and fluorine in aluminosilicate melts at high pressure and high temperature. *American Mineralogist*, *100*(10), 2272–2283.
de Moor, J. M., Kern, C., Avard, G., Muller, C., Aiuppa, A., Saballos, A., et al. (2017). A new sulfur and carbon degassing inventory for the Southern Central American Volcanic Arc: The importance of accurate time-series data sets and possible tectonic processes responsible for temporal variations in arc-scale volatile emissions. *Geochemistry, Geophysics, Geosystems*, *18*, 4437–4468. https://doi.org/10.1002/2017GC007141
Dreyer, B. M., Morris, J. D., & Gill, J. B. (2010). Incorporation of subducted slab-derived sediment and fluid in arc magmas: B-Be-^{10}Be-εNd systematics of the Kuril convergent margin, Russia. *Journal of Petrology*, *51*(8), 1761–1782.
Fedorchenko, V. I., Abdurakhmanov, A. I., & Rodionova, R. I. (1989). *Volcanism of the Kuril Island arc: Geology and petrogenesis*. Moscow, Russia: Nauka.
Fickel, M., & Delgado Granados, H. (2017). On the use of different spectral windows in DOAS evaluations: Effects on the estimation of SO_2 emission rate and mixing ratios during strong emission of Popocatépetl volcano. *Chemical Geology*, *462*, 67–73. https://doi.org/10.1016/j.chemgeo.2017.05.001
Fischer, T. P., Giggenbach, W. F., Sano, Y., & Williams, S. N. (1998). Fluxes and sources of volatiles discharged from Kudryavy, a subduction zone volcano, Kurile Islands. *Earth and Planetary Science Letters*, *160*(1–2), 81–96.
Fischer, T. P., Ramirez, C., Mora-Amador, R., Hilton, D. R., Barnes, J. D., Sharp, Z. D., et al. (2015). Temporal variations in fumaroles gas chemistry at Poas volcano, Costa Rica. *Journal of Volcanology and Geothermal Research*, *294*, 56–70.
Giggenbach, W. (1996). Chemical composition of volcanic gases. In R. Scarpa & R. I. Tilling (Eds.), *Monitoring and mitigation of volcano hazards* (pp. 221–256). Berlin, Germany: Springer.
Giggenbach, W. F. (1987). Redox processes governing the chemistry of fumarolic gas discharges from White Island, New Zealand. *Applied Geochemistry*, *2*(2), 143–161.
Giggenbach, W. F. (1991). Chemical techniques in geothermal exploration. In *Application of geochemistry in geothermal reservoir development* (pp. 119–144). Rome, Italy: United Nations Institute for Training and Research.
Giggenbach, W. F. (1992). Isotopic shifts in waters from geothermal and volcanic systems along convergent plate boundaries and their origin. *Earth and Planetary Science Letters*, *113*(4), 495–510.
Giggenbach, W. F., & Goguel, R. L. (1989). *Collection and analysis of geothermal and volcanic water and gas discharges* (New Zealand DSIR Chem. Div. Rep. 2407, 88 pp.). Christchurch, New Zealand.
Giggenbach, W. F., Shinohara, H., Kusakabe, M., & Ohba, T. (2003). Formation of acid volcanic brines through interaction of magmatic gases, seawater and rock within the White Island volcanic-hydrothermal system, New Zealand. *Society of Economic Geologists Special Publication*, *10*, 19–40.
Gorshkov, G. S. (1970). *Volcanism and upper mantle: Investigation in the Kurile Island arc system*. London, UK: Plenum Press.
Grinenko, V. A., & Thode, H. G. (1970). Sulfur isotope effects in volcanic gas mixtures. *Canadian Journal of Earth Sciences*, *7*(6), 1402–1409.
Halmer, M. M., Schmincke, H. U., & Graf, H. F. (2002). The annual volcanic gas input into the atmosphere, in particular into the stratosphere: A global data set for the past 100 years. *Journal of Volcanology and Geothermal Research*, *115*(3–4), 511–528.
Hilton, D. R., Fischer, T. P., & Marty, B. (2002). Noble gases and volatile recycling at subduction zones. *Noble Gases in Cosmochemistry and Geochemistry*, *47*, 319–370.
Jarrard, R. D. (2003). Subduction fluxes of water, carbon dioxide, chlorine, and potassium. *Geochemistry, Geophysics, Geosystems*, *4*(5), 8905. https://doi.org/10.1029/2002GC000392
Johansson, M., Rivera, C., de Foy, B., Lei, W., Song, J., Zhang, Y., et al. (2009). Mobile mini-DOAS measurement of the outflow of NO_2 and HCHO from Mexico City. *Atmospheric Chemistry and Physics*, *9*(1), 5647–5653. https://doi.org/10.5194/acp-9-5647-2009
Kagoshima, T., Sano, Y., Takahata, N., Maruoka, T., Fischer, T., & Hattori, K. (2015). Sulphur geodynamic cycle. *Scientific Reports*, *5*(1), 8330. https://doi.org/10.1038/srep08330
Kalacheva, E., Taran, Y., & Kotenko, T. (2015). Geochemistry and solute fluxes of volcano hydrothermal systems of Shiashkotan, Kuril Islands. *Journal of Volcanology and Geothermal Research*, *296*, 40–54.
Kalacheva, E., Taran, Y., Kotenko, T., Hattori, K., Kotenko, L., & Solis-Pichardo, G. (2016). Volcano-hydrothermal system of Ebeko volcano, Paramushir, Kuril Islands: Geochemistry and solute fluxes of magmatic chlorine and sulfur. *Journal of Volcanology and Geothermal Research*, *310*, 118–131.
Kalacheva, E., Taran, Y., Voloshina, E., & Inguaggiato, S. (2017b). Hydrothermal system and acid lakes of Golovnin caldera, Kunashir, Kuril Islands: Geochemistry, solute fluxes and heat output. *Journal of Volcanology and Geothermal Research*, *346*, 10–20.

Kalacheva, E. G., Taran, Y. A., Kotenko, T. A., Inguaggiato, S., & Voloshina, E. V. (2017a). The hydrothermal system of Mendeleev Volcano, Kunashir Island, Kuril Islands: The geochemistry and the transport of magmatic components. *Journal of Volcanology and Seismology*, *11*(5), 335–352.

Korzhinsky, M. A., Tkachenko, S. I., Romanenko, I. M., Shteinberg, G. S., & Shmulovich, K. I. (1993). Geochemistry and rhenium mineralization of high-temperature gas flows of the, Kudryavyi volcano, Iturup Kuril Islands [in Russian]. *Doklady Earth Sciences*, *330*(5), 627–629.

Korzhinsky, M. A., Tkachenko, S. I., Shmulovich, K. I., Taran, Y. A., & Steinberg, G. S. (1994). Discovery of a pure rhenium mineral at Kudriavy Volcano. *Nature*, *369*(6475), 51–52.

Kotenko, T. A., Kotenko, L. V., Sandimirova, E. I., Shapar, V. N., & Timofeeva, I. F. (2012). Eruptive activity of Ebeko volcano (Paramushir i.) in 2010–2011 [in Russian]. *Vestnik KRAUNTS*, *1*(19), 160–167.

Mamyrin, B. A., Anufriev, G. S., Kamenskii, I. L., & Tolstikhin, I. N. (1970). Determination of isotopic composition of atmospheric helium. *Geochemistry International*, *7*, 498–505.

Marini, L., Moretti, R., & Accornero, M. (2011). Sulfur isotopes in magmetic-hydrothermal systems, melts and magmas. *Reviews in Mineralogy & Geochemistry*, *73*(1), 423–492.

Markhinin, E. K., & Stratula, D. S. (1977). *Hydrothermal systems of Kuril Islands* (227 pp.) [in Russian]. Moscow, Russia: Nauka.

Martynov, A. Y. (2013). Role of backarc processes in the origin of across arc geochemical zoning in volcanics of early evolutionary stages in Kunashir Island. *Petrology*, *21*(5), 471–506.

Martynov, Y. A., Khanchuk, A. I., Kimura, J.-I., Rybin, A. V., & Martynov, A. Y. (2010). Geochemistry and petrogenesis of volcanic rocks in the Kuril Island arc. *Petrology*, *18* (5), 489–513.

Mather, T. A., Pyle, D. M., Tsanev, V. I., McGonigle, A. J. S., Oppenheimer, C., & Allen, A. G. (2006). A reassessment of current volcanic emissions from the Central American arc with specific examples from Nicaragua. *Journal of Volcanology and Geothermal Research*, *149*(3–4), 297–311.

Melekestsev, I. V., Dvigalo, V. N., & Kirianov, V. Y. (1993). Ebeko volcano (Kuril Islands): History of the eruptive activity and a future volcanic hazard. *Volcanol. Seismol*, *3*, 69–81. (in Russian).

Menyailov, I. A., Nikitina, L. P., & Shapar, V. N. (1985). Results of geochemical monitoring of the activity of Ebeko volcano (Kuril Islands) used for the eruption prediction. *Journal of Geodynamics*, *3*(3–4), 259–274.

Menyailov, I. A., Nikitina, L. P., Shapar, V. N., Rozhkov, A. M., & Miklishansky, A. Z. (1986). Chemical composition and metal content in gas discharges from the 1981 eruption of Alaid volcano, Kuril Islands. *Volcanology and Seismology*, *1*, 26–31.

Quisefit, J. P., Toutain, J. P., Bergametti, G., Javoy, M., Cheynet, B., & Person, A. (1989). Evolution versus cooling of gaseous volcanic emissions from Momotombo volcano, Nicaragua: Thermodynamic model and observations. *Geochimica et Cosmochimica Acta*, *53*(10), 2591–2608.

Rafter, T. A., Wilson, S. H., & Shilton, W. B. (1958). Sulphur isotopic variations in nature, part 6—Sulphur isotopic measurements on the discharge from fumaroles on White Island. *New Zealand Journal of Science*, *1*, 154–171.

Rizzo, A. L., Barberi, F., Carapezza, M. L., Di Piazza, A., Francalanci, L., Sortino, F., et al. (2015). New mafic magma refilling a quiescent volcano: Evidence from He-Ne-Ar isotopes during the 2011–2012 unrest at Santorini, Greece. *Geochemistry, Geophysics, Geosystems*, *16*, 798–814. https://doi.org/10.1002/2014GC005653

Rybin, A. V., Chibisova, M. V., & Degterev, A. V. (2017). Activity of Chirinkotan volcano (Chirinkotan Isl., the Northern Kuriles) in 2013–2016 [in Russian]. *Problems of the Remote Measurements from the Space*, *14*(4), 76–84.

Sano, Y., & Fischer, T. P. (2013). The analysis and interpretation of noble gases in modern hydrothermal systems. In P. Burnard (Ed.), *Noble gases as geochemical tracers* (pp. 249–318). Heidelberg, Germany: Springer.

Sano, Y., & Marty, B. (1995). Origin of carbon in fumarolic gas from island arcs. *Chemical Geology*, *119*(1–4), 265–274.

Sano, Y., & Wakita, H. (1985). Geographical distribution of $^{3}He/^{4}He$ in Japan: Implications for arc tectonics and incipient magmatism. *Journal of Geophysical Research*, *90*(B10), 8729–8741.

Shinohara, H. (2005). A new technique to estimate volcanic gas composition: Plume measurements with a portable multi-sensor system. *Journal of Volcanology and Geothermal Research*, *143*(4), 319–333.

Shinohara, H. (2013). Volatile flux from subduction zone volcanoes: Insights from a detailed evaluation of the fluxes from volcanoes in Japan. *Journal of Volcanology and Geothermal Research*, *268*, 46–63.

Shinohara, H., Giggenbach, W. F., Kazahaya, K., & Hedenquist, J. W. (1993). Geochemistry of volcanic gases and hot springs of Satsuma Iwojima, Japan. *Geochemical Journal*, *27*(4/5), 271–285.

Stern, R. G. (2002). Subduction zones. *Reviews of Geophysics*, *40*(4), 1012. https://doi.org/10.1029/2001RG000108

Stratula, D. S. (1969). *Volcanoes and hot springs of Shiashkotan Island* (PhD thesis) [in Russian]. Petropavlovsk-Kamchatsky, Russia: Institute of Volcanology.

Symonds, R. B., Gerlach, T. M., & Reed, M. H. (2001). Magmatic gas scrubbing: Implications for volcano monitoring. *Journal of Volcanology and Geothermal Research*, *108*(1–4), 303–341.

Symonds, R. B., & Reed, M. H. (1993). Calculation of multicomponent chemical equilibria in gas-solid-liquid systems: Calculation method, thermochemical data and applications to studies of high-temperature gases with example from Mount St. Helens. *American Journal of Science*, *293*(8), 758–864.

Tamburello, G. (2015). Ratiocalc: Software for processing data from multicomponent volcanic gas analyzers. *Computers & Geosciences*, *82*, 63–67. https://doi.org/10.1016/j.cageo.2015.05.004

Taran, Y. (1992). Chemical and isotopic composition of fumarolic gases from Kamchatka and Kurile Islands. *Reports, Geological Survey of Japan*, *279*, 183–186.

Taran, Y. A. (2009). Geochemistry of volcanic and hydrothermal fluids and volatile budget of the Kamchatka–Kuril subduction zone. *Geochimica et Cosmochimica Acta*, *73*(4), 1067–1094.

Taran, Y. A. (2011). N_2, Ar and He as a tool for discrimaneting sources of volcanic fluids with application to Vulcano, Italy. *Bulletin of Volcanology*, *73*(4), 395–408.

Taran, Y. A., Bernard, A., Gavilanes, J.-C., Lunezheva, E., Cortes, A., & Armienta, M. A. (2001). Chemistry and mineralogy of high-temperature gas discharges from Colima volcano, Mexico. Implications for magmatic gas–atmosphere interaction. *Journal of Volcanology and Geothermal Research*, *108*(1–4), 245–264. https://doi.org/10.1016/S0377-0273(00)00289-4

Taran, Y. A., Connor, C. B., Shapar, V. N., Ovsyannikov, A. A., & Bilichenko, A. A. (1997). Fumarolic activity of Avachinsky and Koryaksky volcanoes, Kamchatka, from 1993 to 1994. *Bulletin of Volcanology*, *58*(6), 441–448.

Taran, Y. A., Gavrilenko, G. M., Chertkova, L. V., & Grichuk, D. V. (1993). A geochemical model for the hydrothermal system of Ushishir Volcano, Kuril Islands. *Volcanology and Seismology*, *1*, 55–68.

Taran, Y. A., Hedenquist, J. W., Korzhinsky, M. A., Tkachenko, S. I., & Shmulovich, K. I. (1995). Geochemistry of magmatic gases of Kudryavy volcano, Iturup, Kuril islands. *Geochimica et Cosmochimica Acta*, *59*(9), 1749–1761.

Taran, Y. A., Pokrovsky, B. G., & Doubik, Y. M. (1989). Isotopic composition and origin of water in andesitic magmas. *Doklady Earth Sciences*, *304*, 1191–1194.

Taran, Y. A., Pokrovsky, B. G., & Volynets, O. N. (1997). Hydrogen isotopes in hornblendes and biotites from uaternary volcanic rocks of the Kamchatka-Kurile arc. *Geochemical Journal*, *31*(4), 203–221.

Taran, Y., & Zelenski, M. (2014). Systematics of water isotopic composition and chlorine content in arc-volcanic gases. In G. F. Zellmer, M. Edmonds, & S. M. Straub (Eds.), *The role of volatiles in the genesis, evolution and eruption of arc magmas. Geological Society, London, Special Publications* (pp. 410–432).

Taylor, B. E. (1986). Magmatic volatiles: Isotopic variation of C, H, and S. *Reviews in Mineralogy and Geochemistry*, *16*, 185–225.

Tkachenko, S. I., Taran, Y. A., Korzhinsky, M. A., Pokrovsky, B. G., Steinberg, G. S., & Shmulovich, K. I. (1992). Gas jets of Kudryavy volcano, Iturup Island, Kurils. *Transactions (Doklady) of the Russian Academy of Sciences USSR*, *325*, 823–826.

Van Soest, M. C., Hilton, D. R., Macpherson, C. G., & Mattey, D. P. (2002). Resolving sediment subduction and crustal contamination in the Lesser Antilles Island arc: A combined He-O-Sr isotope approach. *Journal of Petrology*, *43*(1), 143–170.

Wahrenberger, C., Seward, T. M., & Dietrich, V. (2002). Volatile traceelement transport in high-temperature gases from Kudryavy volcano (Iturup, Kurile Islands, Russia). In R. Hellmann & S. A. Wood (Eds.), *Water–rock interaction: A TRIBUTE TO David A. Crerar. Geochemical Society Special Publications* (Vol. 7, pp. 307–327).

Yudovskaya, M. A., Tessalina, S., Distler, V. V., Chaplygin, I. V., Chugaev, A. V., & Dikov, Y. P. (2008). Behavior of highly-siderophile elements during magma degassing: A case study at the Kudryavy volcano. *Chemical Geology*, *248*(3–4), 318–341.

Zelenski, M., Malik, N., & Taran, Y. (2014). Emissions of trace elements during the 2012–2013 effusive eruption of Tolbachik volcano, Kamchatka: Enrichment factors, partition coefficients and aerosol contribution. *Journal of Volcanology and Geothermal Research*, *285*, 136–149.

Zelenski, M. E., Kamenetsky, V. S., & Hedenquist, J. W. (2016). Gold recycling and enrichment beneath volcanoes: A case study of Tolbachik, Kamchatka. *Earth and Planetary Science Letters*, *437*, 35–46.